https://doi.org/10.5194/tc-2022-223
Preprint. Discussion started: 1 December 2022

The Cryosphere Discussions

Observed and modeled Greenland firn properties (1980–2020)

Megan Thompson-Munson[1], Nander Wever[1], C. Max Stevens[2], Jan T. M. Lenaerts[1], and Brooke Medley[2,3]

[1]Department of Atmospheric and Oceanic Sciences, University of Colorado Boulder, Boulder, CO, USA
[2]Earth System Science Interdisciplinary Center, University of Maryland College Park, College Park, MD, USA
[3]NASA Goddard Space Flight Center, Greenbelt, MD, USA

Correspondence: Megan Thompson-Munson (megan.thompson-munson@colorado.edu)

Abstract. The Greenland Ice Sheet's (GrIS) firn layer buffers the ice sheet's contribution to sea level rise by storing meltwater in its pore space. However, available pore space and meltwater retention capability is lost due to ablation of the firn layer and refreezing of meltwater as near-surface ice slabs in the firn. Understanding how firn properties respond to climate is important for constraining the GrIS's future contribution to sea level rise in a warming climate. Observations of firn density provide detailed information about firn properties, but they are spatially and temporally limited. Here we use two firn models, the physics-based SNOWPACK model and the semi-empirical Community Firn Model (CFM) to quantify firn properties across the GrIS from 1980 through 2020. We use an identical forcing (MERRA-2 atmospheric reanalysis) for SNOWPACK and the CFM in order to isolate model differences. To evaluate the models, we compare simulated firn properties, including firn air content (FAC), to measurements from the SUMup dataset of snow and firn density. Both models perform well, though their performance is hindered by meltwater percolation and the spatial resolution of the atmospheric forcing. In the full ice-sheet simulations, the spatially-integrated FAC (i.e., air volume in the firn) for the upper 100 m is 34,645 km^3 from SNOWPACK and 28,581 km^3 from the CFM. The discrepancy in the magnitude of the modeled FAC stems from differences in densification with depth and variations in the models' treatment of atmospheric input. In more recent years (2005–2020), both models simulate substantial depletion of pore space. During this period, the spatially-integrated FAC across the entire GrIS decreases by 2.8 % and 1.2 % in SNOWPACK and the CFM, respectively. The differing magnitudes of the 2005–2020 spatially-integrated FAC of -66.6 km^3 yr^{-1} in SNOWPACK and -17.4 km^3 yr^{-1} in the CFM demonstrate how model differences propagate throughout the FAC record. Over the full modeled record (1980–2020), SNOWPACK simulates a loss of pore space equivalent to 3 mm of sea level rise buffering, while the CFM simulates a loss of 1 mm. The greatest depletion in FAC is along the margins, and especially along the western margin where observations and models show the formation of near-surface, low-permeability ice slabs that inhibit meltwater storage.

https://doi.org/10.5194/tc-2022-223
Preprint. Discussion started: 1 December 2022


The Cryosphere Discussions

1 Introduction

Most of the Greenland Ice Sheet (GrIS) is covered in a thick, porous layer of partially compacted snow known as firn. The density of firn varies across the ice sheet and is sensitive to surface mass balance (SMB) processes like accumulation and melt, which cause firn density to also vary in time and on several different temporal scales (e.g., daily, seasonal, annual). Since firn is porous, it is capable of storing meltwater in its pore space in a solid or liquid form, which can buffer sea-level rise (Harper et al., 2012). Meltwater can remain in a liquid form and remain near the surface in weathered ice crusts (Cooper et al., 2018), pool into subsurface lakes (Dunmire et al., 2021), or percolate into the snowpack and remain in a liquid form in firn aquifers (e.g., Forster et al., 2014). Additionally, meltwater can percolate into the snowpack where it refreezes deeper in the firn layer or is stored in the firn's pore space (Pfeffer et al., 1991; Harper et al., 2012). Refreezing of meltwater within the firn frequently occurs and creates ice lenses (<0.1 m thick) and layers (0.1-1 m thick) that can accumulate into low-permeability ice slabs (>1 m thick) (MacFerrin et al., 2022). These ice slabs make deeper pore space inaccessible to meltwater produced at the surface, which reduces the buffering capacity of the firn (Machguth et al., 2016) and increases the elevation below which meltwater runs off (Tedstone and Machguth, 2022). Rapid depletion of the pore space on the GrIS is expected to accelerate mass loss in the 21st century and increase the ice sheet's contribution to sea level rise (van Angelen et al., 2013). Approximately half of GrIS mass loss is due to an increase in meltwater runoff (van den Broeke et al., 2009; Enderlin et al., 2014), making the firn's buffering capacity increasingly important to the GrIS contribution to sea-level rise.

In recent decades, Greenland's firn layer has begun to show evidence of climate change. The 2012 extreme melt season produced expansive ice slabs that persisted for several years and reduced permeability (Culberg et al., 2021). At lower elevations, where significant melt occurs, firn has lost its capacity to store meltwater (Machguth et al., 2016). In higher-elevation areas where less meltwater is generated, the firn structure has still changed through enhanced densification from warmer temperatures and the presence of liquid water (Machguth et al., 2016), which causes ice-sheet surface height lowering (de la Peña et al., 2015). Changes in the amount of air-filled pore space within the firn, known as the firn air content (FAC), have been investigated in both observations (e.g., Vandecrux et al., 2019) and models (e.g., Medley et al., 2022). Although regeneration of this pore space is slow (Harper et al., 2012), consecutive years of average or below-average melt have shown to temporarily pause FAC depletion (Rennermalm et al., 2021). These complex interactions between melt and pore space depletion, including the memory effect of changes to the firn from previous years, motivate the use of detailed firn models to capture these processes and to enhance our understanding of the changes occurring in the firn.

Modeling firn has become important for estimating mass balance (MB) from satellite altimetry, since this method relies on firn models to interpret the causes of surface height changes (e.g., Li and Zwally, 2011). Changes in surface height cannot be attributed to ice mass or firn density changes without additional information from firn models (Smith et al., 2022). Accurate estimates of ice sheet firn density over time and space are necessary to constrain the uncertainty in MB assessments relying on surface height changes measured in satellite altimetry. Additionally, understanding the limits and deficiencies in firn models is essential for quantifying uncertainties in altimetry-based MB estimates.

https://doi.org/10.5194/tc-2022-223
Preprint. Discussion started: 1 December 2022

Firn models can also be used to fill in gaps in firn density observations and study how firn properties vary on larger spatial and temporal scales, especially since in-situ and remotely sensed observations can only provide snapshots of firn properties in space and time. Semi-empirical firn models have been used to simulate firn properties on both Greenland (e.g., Medley et al., 2022) and Antarctica (e.g., Ligtenberg et al., 2011). These models use empirical relationships between densification, accumulation, and temperature, and they are often tuned to observations (e.g., Ligtenberg et al., 2011; Medley et al., 2022; Li and Zwally, 2011). Semi-empirical models are beneficial because they do not rely on the physics of firn densification, which are not fully understood. On the other hand, the observations these models rely on for calibration may not be representative of future firn properties in a warming climate (Ligtenberg et al., 2018). Additionally, these models are often tuned using depth-density profiles, which requires a steady-state assumption and thereby lends uncertainty in their ability to simulate firn changes in a transient climate (Lundin et al., 2017). The alternatives to semi-empirical models are physics-based models that use the constitutive relationship between stress and strain for snow to simulate densification (e.g., Vionnet et al., 2012; Bartelt and Lehning, 2002; Lehning et al., 2002a, b). While physics-based models do not rely on observations from tuning, they generally need more detailed meteorological forcing data and are limited by uncertainties in physical processes. Physics-based models are typically developed to simulate seasonal snow processes rather than firn processes since snow physics have been more-thoroughly studied. Still, both semi-empirical as well as physics-based firn models have been successfully used in Greenland (e.g., Vandecrux et al., 2020b; Dunmire et al., 2020; Medley et al., 2022).

The semi-empirical Community Firn Model (CFM) and physics-based SNOWPACK firn model have seen significant development for polar regions in recent years (e.g., Medley et al., 2022; Keenan et al., 2021; Stevens et al., 2020). At an ice-sheet scale, few comparisons of semi-empirical and physics-based models exist. In many studies investigating firn models, only a single atmospheric forcing is used with a single model (e.g., Medley et al., 2022). Reported results are often not directly comparable between studies since statistics are calculated over different spatial extents or time periods. This approach makes it difficult to attribute differences between modeled and observed firn properties to model forcing (i.e., boundary conditions) or the model itself (i.e., the representation of physical processes by the model).

Here we use the CFM and SNOWPACK to simulate firn properties on the GrIS. Importantly, we use the same atmospheric forcing for both models in order to identify model differences that are completely independent from the forcing data. We compare the simulated firn properties to point observations and then extend the model domain to the entire ice sheet and simulate evolving firn properties across Greenland from 1980 through 2020. In Section 2, we describe the methods used and include descriptions of the firn models, atmospheric forcing, and observational dataset. Section 3 reports the results, which we partition into the model evaluation (Section 3.1), a description of firn properties in a steady state climate (Section 3.2), and a description of firn properties in a changing climate (Section 3.3).

https://doi.org/10.5194/tc-2022-223
Preprint. Discussion started: 1 December 2022


The Cryosphere Discussions

2 Methods

2.1 MERRA-2 atmospheric forcing

The Modern-Era Retrospective Analysis for Research and Applications, version 2 (MERRA-2) is a global atmospheric reanalysis spanning the period from 1980 to present day (Gelaro et al., 2017). We use MERRA-2's hourly 2-m air temperature, relative humidity, 10-m wind speed, incoming shortwave radiation, incoming longwave radiation, and precipitation rate for the 1980–2020 period (Global Modeling and Assimilation Office (GMAO), 2015a, b, c, d) to force both firn models. MERRA-2 is a gridded product with a horizontal resolution of 0.5° latitude by 0.625° longitude. Due to convergence of meridians toward the poles, the MERRA-2 grid becomes more tightly spaced at higher latitudes. To account for this, we weight model grid points by the cosine of the latitude when calculating ice-sheet-wide or basin-wide averages of firn and atmospheric properties. We choose to use MERRA-2 since it is publicly available, regularly updated and released, and spans a temporal window that captures recent climate change (Fig. A2). Regional climate models are not always widely available or regularly updated, and no single reanalysis clearly outperforms others over the GrIS (Zhang et al., 2021). Additionally, our focus is comparing two firn models with the same forcing in order to isolate model differences. As such, the choice of the forcing dataset is less important for the interpretation of our results.

In order to evaluate and compare the firn models, we first run them using forcing data from only the grid cells nearest to firn density observations. We use 177 MERRA-2 grid cells for this first step. For the full ice-sheet simulations, we mask out gird cells with an ice coverage of less than 50 %, which leaves us with a model domain of 1784 MERRA-2 grid cells. The total area of the model domain is 1.81 million km^2, which is greater than the actual ice-sheet area of 1.71 million km^2 (Rignot and Mouginot, 2012).

2.2 SNOWPACK firn model

SNOWPACK is a single-column, physics-based, multi-layer snow and firn model originally designed for avalanche warning in alpine environments (Bartelt and Lehning, 2002; Lehning et al., 2002a, b). In recent years, this model has been successfully applied over the GrIS (e.g., Van Tricht et al., 2016; Steger et al., 2017; Izeboud et al., 2020; Dunmire et al., 2021), as well as the Antarctic Ice Sheet (Dunmire et al., 2020; Keenan et al., 2021). It uses a Lagrangian framework and adds layers when snowfall occurs with a new-snow density based on atmospheric conditions (e.g., Keenan et al., 2021), including explicit treatment of the wind compaction under drifting and blowing snow conditions (Wever et al., 2022). Firn densification is calculated using the constitutive relationship between stress and strain in snow (Bartelt and Lehning, 2002; Lehning et al., 2002a). For calculating firn temperatures, the upper boundary condition is determined from a surface energy balance scheme. The model describes snow microstructure based on four parameters: grain radius, bond radius, sphericity, and dendricity. These evolve over time primarily based on temperature, temperature gradients, and liquid water content (Lehning et al., 2002a). SNOWPACK uses the MeteoIO library (Bavay and Egger, 2014) for preparing the meteorological forcing data for the simulations.

We run SNOWPACK with half-hourly time steps. To conserve computational expenses and keep model output sizes manageable, detailed model output for all firn layers is stored with 7-day temporal resolution. SNOWPACK's simulated firn layers

https://doi.org/10.5194/tc-2022-223
Preprint. Discussion started: 1 December 2022

have variable thicknesses, impacted by the layer-merging scheme use to reduce computational cost. However, higher vertical resolution of a few centimeters per layer is maintained in the near-surface layers where the firn is more sensitive to short-term atmospheric fluctuations. We set the surface roughness to 0.002 m for solving the energy balance with the Michlmayr et al. (2008) stability correction when a stable boundary layer is diagnosed.

Since the thickness of the firn layer varies and we aim to simulate processes for the full firn column depth, we spin up the model to build a firn layer until a thickness of at least 150 m is reached, or when the bottom 3 m of the simulated firn consist of solid ice with a total thickness of at least 10 m (whichever condition is reached first). To perform the spin-up, we run the model using forcing data from a reference climate interval (RCI) and repeat the model runs until the desired thickness is reached. Once reached, we perform a final model run using the full-length record (1980–2020). We choose an RCI of 1 January 1980 through 31 December 1995, which is the same period used in Medley et al. (2022). We make the assumption that this period is representative of the longer-term Greenland climate.

2.3 The Community Firn Model (CFM)

The Community Firn Model (CFM, Stevens et al., 2020) is an open-source model framework that simulates the evolution of firn. It is designed to be modular, allowing the model user to choose which physical processes to simulate in a given model run. The core CFM modules simulate firn density and temperature evolution as well as meltwater refreezing and runoff. Additionally, the user can easily choose different parameterizations to use for a particular model run, including the firn-densification equation, thermal conductivity, surface density, and water percolation scheme. Like SNOWPACK, the CFM uses a Lagrangian numerical framework; each accumulation event adds a new layer to the grid and one is removed from the bottom. The CFM uses a layer-merging scheme at 5- and 10-m depth to reduce computational demands. Model outputs are interpolated onto a 0.25-m regular grid to reduce output file size.

For the present work, we run the CFM over the GrIS at daily resolution. The CFM's required forcing inputs for these model runs are surface temperature, precipitation (rain and snow), sublimation, and melt. However, MERRA-2 does not explicitly provide a melt flux. As such, we force the CFM with outputs from SNOWPACK's surface energy balance scheme, including skin temperature, melt flux, and sublimation. This method ensures that the surface boundary conditions (i.e., mass and energy fluxes) for the CFM and SNOWPACK model runs are consistent.

The CFM is modular and offers the user several parameterization choices, but in this work we select a single configuration for all model runs. We use a constant surface density of 350 kg m^{-3} for the CFM runs, which is a reasonable estimate when compared to observed and SNOWPACK-modeled surface density (Fig. A1). The densification rate is determined with the NASA GSFC-FDMv1 firn densification equation (Medley et al., 2022). This equation is based on the firn densification equation proposed by Arthern et al. (2010), but optimized using firn-core data from 226 sites across the Antarctic and Greenland Ice Sheets. We use a bucket scheme with an enthalpy-based heat flow module to handle meltwater percolation and refreezing.

The simulations for each grid cell are initialized with a depth/density profile predicted by the Herron and Langway (1980) steady state model. The depth of the model domain varied for each grid cell but was chosen to be near the depth at which the firn reaches the ice density. We design the CFM spin-up to repeat the RCI of 1980–1995 until the entire initial firn column is

https://doi.org/10.5194/tc-2022-223
Preprint. Discussion started: 1 December 2022

refreshed. For example, if the firn needs 1000 years to spin up, the RCI would repeat 63 times. Once the spin up is completed, the main model run (1980–2020) commences.

2.4 SUMup observations

The Surface Mass Balance and Snow on Sea Ice Working Group (SUMup) dataset is a compilation of Arctic and Antarctic observations of SMB components and includes in-situ observations of firn density on both ice sheets (Montgomery et al., 2018). The 2022 SUMup release contains data from 845 locations in Greenland (Thompson-Munson et al., 2022) that we use to compare with modeled firn properties. The measurements have been taken over the past several decades and the depths of the cores range from 0.03 m to 334.53 m. Of the 845 measurements, 78 are single point measurements of surface density only. For calculating depth-integrated properties, we only use the 767 observations that contain data points from at least two different depths.

2.5 Firn air content (FAC) calculation

To compare the observations with the model results, we select the modeled density profile from the closest location and date to when the measurement was taken. The CFM produces daily output, which means the observed and model date are the same. SNOWPACK output for the model evaluation is weekly, which means that the date of the modeled profile can differ from the date of the observed profile by as much as 3 days.

From the observed and modeled density profiles, we calculate the FAC (also known as "depth-integrated porosity (DIP)"), which has units of meters. The FAC is a quantification of the air-filled pore space in the firn. For any depth interval from z_j (upper bound) to z_k (lower bound) where z = 0 m represents the surface, the FAC is calculated as

$$FAC(z_k - z_j) = \int_{z_j}^{z_k} \frac{\rho_{ice} - \rho(z)}{\rho_{ice}} \, dz \tag{1}$$

where ρ_{ice} is the density of ice (917 kg m^{-3}) and $\rho(z)$ is the layer density at a given depth.

To evaluate the firn models and ensure a direct comparison with the observations, we first calculate the FAC only over the depths represented by the observations (Section 3.1). For these comparisons, z_j is the uppermost observation depth and z_k is the lowermost observation depth. When examining ice-sheet-wide firn properties (Sections 3.2 and 3.3), we calculate FAC from the surface to a depth of 100 m (z_j = 0 m, z_k = 100 m), and for 10-m-thick vertical intervals from 0 m down to 50 m (z_j = 0, 10, 20, 30, 40 m; z_k = 10, 20, 30, 40, 50 m).

2.6 Metrics of model evaluation

We use several metrics to compare the modeled density and FAC to the observations in order to evaluate model performance. The Nash-Sutcliffe efficiency (NSE) coefficient is a measure of a model's goodness of fit and is typically employed in hydro-

https://doi.org/10.5194/tc-2022-223
Preprint. Discussion started: 1 December 2022

logical modeling (NSE; Nash and Sutcliffe, 1970). It is calculated as

$$NSE = 1 - \frac{\sum_{i=1}^{n}(O_i - M_i)^2}{\sum_{i=1}^{n}(O_i - \overline{O})^2} \tag{2}$$

where O_i is the observation value, M_i is the model value, $\overline{O}$ is the observation mean, and n is the number of values. For quantifying the accuracy of the models, we use the mean absolute percentage error (MAPE), which is calculated as

$$MAPE = \frac{1}{n}\sum_{i=1}^{n}\left|\frac{O_i - M_i}{O_i}\right| \times 100\% \tag{3}$$

Finally, we use the relative bias to understand the fractional degree of under- or over-estimation of the models. At each observation location, we calculate relative bias as

$$Relative\ bias_i = \frac{M_i - O_i}{O_i} \times 100\% \tag{4}$$

and for the full set of locations, we calculate a single, bulk bias value as

$$Bulk\ relative\ bias = \frac{\sum_{i=1}^{n}(M_i - O_i)}{\sum_{i=1}^{n}(O_i)} \times 100\% \tag{5}$$

3 Results

3.1 Model evaluation

Since we use two models in this study, we first discuss the shared and distinct features in simulated density profiles for two example observations from the SUMup database (Wilhelms, 2000; Machguth et al., 2016). Figure 1a compares a 16.3-m-deep core with several ice layers collected in southwest Greenland (gray, Machguth et al., 2016) to model results from SNOWPACK (blue) and the CFM (green). In this example, both SNOWPACK and the CFM simulate high-density layers ∼1 m below the surface that form as a result of high melt in 2012. The observed profile also reaches high densities (>700 kg m^{-3}) near the surface. However, neither model captures the even higher-density observed ice layer (>800 kg m^{-3}) at ∼5 m depth. The models show higher agreement with one another in the surface and begin to diverge with depth. SNOWPACK simulates more variability between layers compared to the CFM. This partly results from the fixed surface density of 350 kg m^{-3} set for the CFM, while the surface density in SNOWPACK varies based on atmospheric conditions, and partially because the CFM outputs are interpolated onto a grid. For polar regions in particular, temporal variations in wind and the presence of drifting snow translate into vertical density variations with increasing accumulation. Figure 1b compares a 102.4-m-deep core from the high-elevation interior measured with gamma-ray attenuation (Wilhelms, 2000) with outputs from both models. The modeled profile shapes generally match the observed profile with an NSE of 0.96 for both SNOWPACK and the CFM (Fig. 1b). SNOWPACK's inter-layer variability is present in the upper ∼25 m and matches the degree of variability seen in the observations. SNOWPACK's density variability stems from the effect of microstructure on the settling, which disappears at depth due to the model's layer merging algorithm.

https://doi.org/10.5194/tc-2022-223
Preprint. Discussion started: 1 December 2022

Since most observations are from shallow cores (median depth = 2.0 m; Fig. 2a) the observed FAC values are relatively low (median FAC = 1.3 m; Fig. 2b) and do not represent the FAC of the full firn column. Generally, modeled FAC from both SNOWPACK and the CFM agree very well with the calculated FAC from the observed density profiles (Fig. 3). The NSE is 0.90 for SNOWPACK and 0.94 for the CFM, and the MAPE is 14 % for SNOWPACK and 16 % for CFM (Fig. 3). The bulk relative biases of +7.9 % for SNOWPACK and +0.2 % for the CFM show that both models are overestimating FAC (Fig. 2c, d), though this overestimation is not statistically significant (p = 0.13 for SNOWPACK, p = 0.49 for the CFM). For both models, the relative bias calculated at each observation site is less than 10 % for the majority of points (69 % of SNOWPACK points and 64 % of the CFM points). Only 2 % of points in SNOWPACK and 1 % of points in the CFM have relative biases greater than 100 %. Many of the large biases occur along the margins of the ice sheet, particularly in the southeast and southwest (Fig. 2c, d).

For both models, five of the highest absolute biases occur in five cores located in the same MERRA-2 grid cell (Fig. 4). The grid cell is located in an area with observed firn aquifers (Miller et al., 2018), and it contains large topographic gradients. Here, the models use the same MERRA-2 climatology to simulate firn properties for five observations. Both SNOWPACK and the CFM overestimate FAC; absolute biases exceed 5 m and relative biases exceed 100 % in all but one of these cases (Fig. 3, 4). Within this grid cell, the observations substantially differ from the models, especially as the distance between the center of the MERRA-2 grid cell and the observation location increases. The biases are highest furthest from the grid cell center and where the topography is steepest (Fig. 4).

3.2 Firn properties in a steady-state climate

In this section we compare the modeled results over the entire GrIS during the RCI. The RCI used for model spin-up spans 1980 through 1995, and since we assume that this period represents a relatively steady-state, long-term Greenland climate (Fig. A2), the modeled firn is considered to be in steady state as well. This RCI has been used previously by Medley et al. (2022). Since the forcing data from SNOWPACK and the CFM are identical, differences in the simulated firn properties can be directly attributed to the differences between models. We calculate FAC for the upper 100 m of the firn column in both SNOWPACK and the CFM to reduce any possible biases arising from inconsistent maximum depths between the two models. Unless otherwise stated, all FAC values reported in the remainder of the manuscript have been calculated for the upper 100 m. Additionally, when calculating spatial means in FAC, we weight the values to account for the converging meridians that lead to variable sizes of MERRA-2 grid cells.

We use the liquid-to-solid ratio (LTSR) averaged over the RCI to investigate how both models respond to liquid water input from snowmelt and rain, and solid input from accumulation in a relatively steady state climate. The LTSR is calculated as

$$LTSR = \frac{melt + rain}{snow} \tag{6}$$

and is the same for SNOWPACK and the CFM since they use the same forcing data. Overall, the range of SNOWPACK FAC is greater than the range of the CFM FAC (Fig. 5a). At very low LTSR values (<0.10) where snowfall is the dominant component of surface mass fluxes, FAC in SNOWPACK ranges from 9.7 to 32.1 m, whereas FAC in the CFM ranges from 9.9 to only

https://doi.org/10.5194/tc-2022-223
Preprint. Discussion started: 1 December 2022

The Cryosphere Discussions
Open Access
EGU

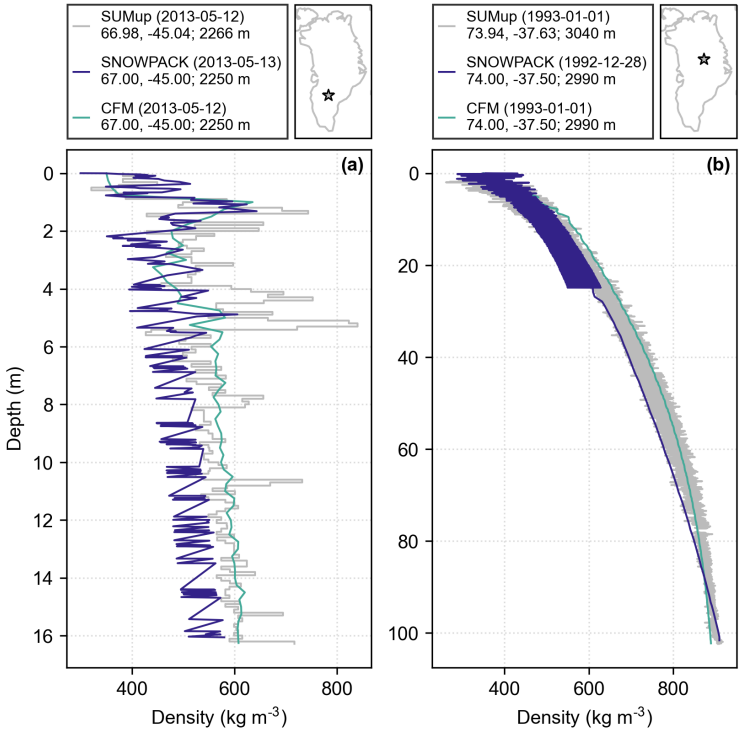

Figure 1. Modeled and observed density profiles at two example locations from (a) Machguth et al. (2016) and (b) Wilhelms (2000). The locations of the observations are shown as stars on the map and the profile dates, latitudes, longitudes, and elevations for the observations and models are reported in the legends. Observations are shown in gray, SNOWPACK results are in blue, and the CFM results are in green.

23.6 m. As the LTSR increases and liquid input dominates, the FAC in both models approaches zero. However, SNOWPACK FAC decreases more rapidly and reaches lower FAC values than the CFM at high LTSR values. The CFM FAC decreases more gradually with increasing LTSR. In SNOWPACK, 127 points have an FAC less than 1 m, and in the CFM only 2 points are as low (Fig. 5a). We also examine how FAC responds to the summer (June, July, and August) 2-m air temperature during the RCI (Fig. 5b). For summer temperatures below ∼-4°C, both models consistently simulate the FAC values exceeding 10 m. For these low temperatures, the range of FAC is greater in SNOWPACK (9.9 to 32.1 m) compared to the CFM (10.7 to 23.5 m). Both models show a rapid decline in FAC as summer temperatures exceed -4°C, and the modeled response is similar at these warmer temperatures.

During the RCI, SNOWPACK and the CFM produce generally similar spatial patterns in FAC across the ice sheet, though the magnitudes differ (Fig. 6). SNOWPACK simulates an FAC of 19.1±8.0 m (mean±standard deviation) and the CFM simulates an FAC of 15.8±6.0 m, which constitutes a 19 % difference (Fig. 6; Table 1). We also calculate FAC for vertical segments in steps of 10-m for the ice sheet from a depth of 0 m (surface) down to 50 m (Fig. 7). In both models, the FAC is highest in the shallowest segment (closest to the surface) and lowest in the deepest segment, consistent with densification. In each vertical

https://doi.org/10.5194/tc-2022-223
Preprint. Discussion started: 1 December 2022

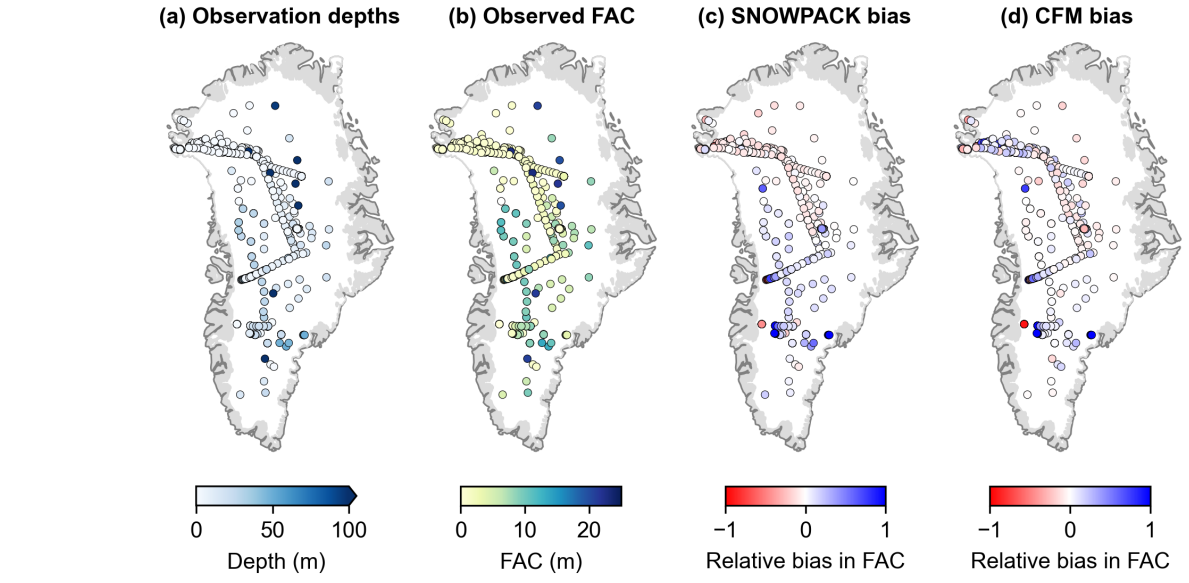

Figure 2. (a) Locations of the 767 SUMup cores used for analysis with shading indicating the depth of the core. (b) Firn air content (FAC) calculated from the observed densities in SUMup. (c) Relative bias between SNOWPACK-modeled FAC and observed FAC. (d) Relative bias between the CFM-modeled FAC and observed FAC. Positive bias indicates an overestimation of FAC by the model, while negative bias indicates an underestimation of FAC by the model.

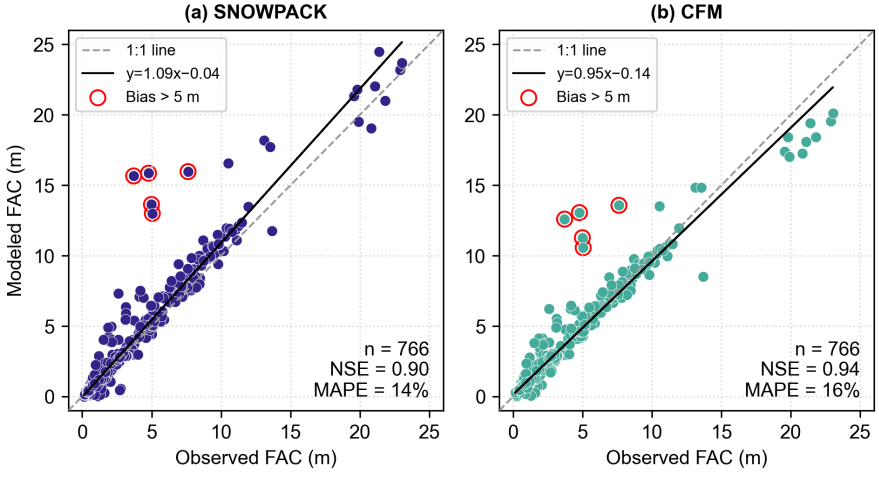

Figure 3. Observed versus modeled firn air content (FAC) for (a) SNOWPACK and (b) the CFM. The number of points (n), the Nash-Sutcliffe Efficiency (NSE), and the mean absolute percentage error (MAPE) are reported for each model in the lower right. The gray dashed line is a 1:1 line, and the black solid line is the linear regression. Points with biases greater than 5 m are circled in red and correspond to the density profiles shown in Figure 4.

https://doi.org/10.5194/tc-2022-223
Preprint. Discussion started: 1 December 2022

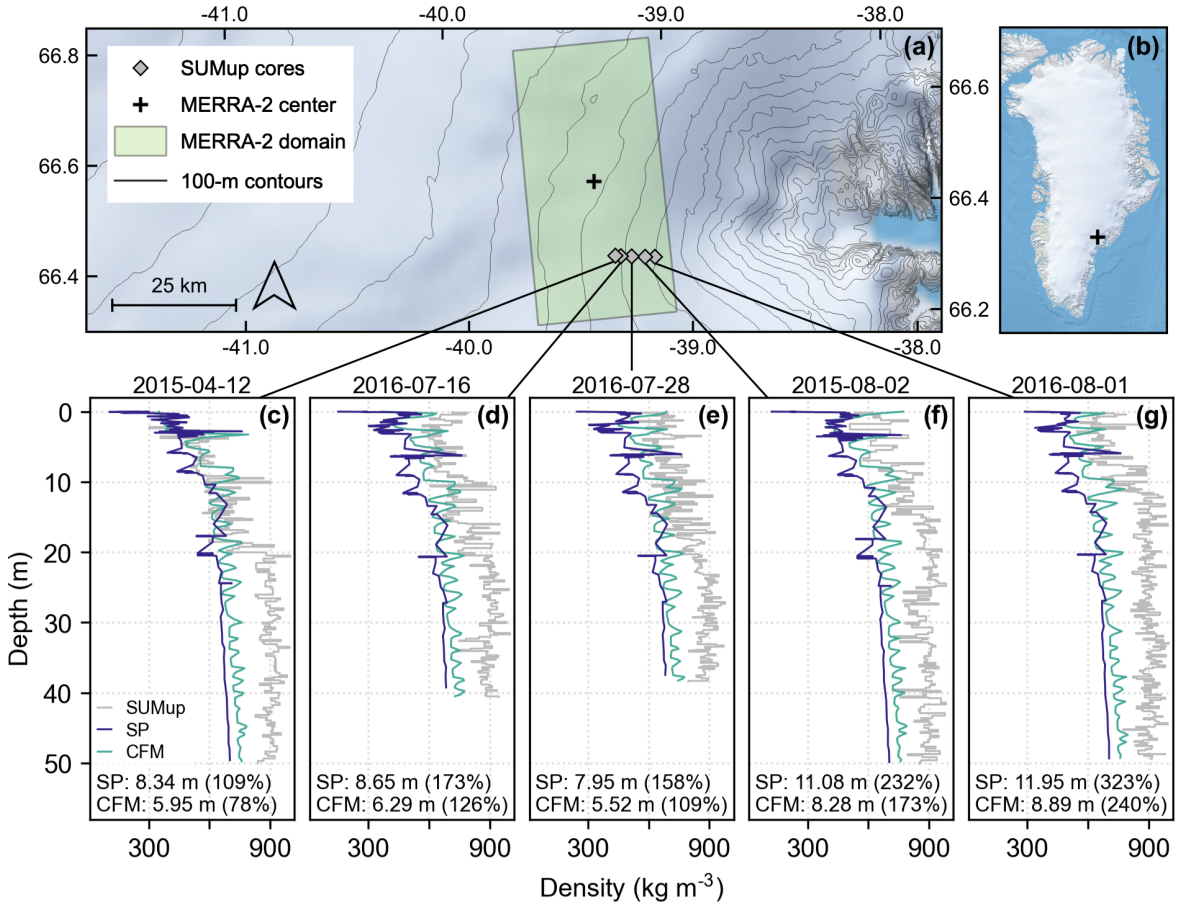

Figure 4. Density profiles and locations of high model biases from Fig. 3. (a) Map showing the five SUMup cores plotted in (c-g), the MERRA-2 domain used for SNOWPACK and the CFM simulations shown in (c-g), and 100-m surface elevation contours from the BedMachine dataset (Morlighem et al., 2017). (b) Location map of Greenland with the black plus sign indicating the region shown in (a). Maps in panels (a) and (b) were created with QGreenland v2.0.0 (Moon et al., 2022). (c-g) Observed and modeled density profiles for five locations in southeast Greenland where both SNOWPACK and the CFM overestimate firn air content by at least 5 m. The modeled profiles come from the same simulation for the MERRA-2 grid point closest to the firn cores, but differ in date and time to match the observation date as closely as possible. In each panel, we report the FAC absolute bias (modeled minus observed) and the relative bias (in parentheses) for SNOWPACK ("SP") and the CFM.

https://doi.org/10.5194/tc-2022-223
Preprint. Discussion started: 1 December 2022

segment, the SNOWPACK FAC is greater than the CFM FAC, but the percent difference between the models increases with depth. The models produce similar FAC values between 0 and 10 m, with a difference of 7 %. However, from 40 to 50 m depth, there is a 29 % difference between SNOWPACK and the CFM (Fig. 7).

To better understand spatial patterns represented by both models, we compare FAC in each basin of the GrIS as defined by Rignot and Mouginot (2012). The six basins and their abbreviations used in subsequent figures and tables are the northwest (NW), central west (CW), southwest (SW), north (NO), northeast (NE), and southeast (SE). These basins have distinct climatological features captured by MERRA-2 (Table A1). The southeast and southwest are the warmest and wettest basins as they have the highest temperatures, melt, and precipitation. The precipitation in the southeast is substantially higher (>37 %) than in any other basin. The coldest and driest basins are the north and northeast, which are characterized by very low temperatures, melt, and precipitation. Lastly, the central west and northwest basins fall in the middle with moderate amounts of precipitation and melt but relatively low temperatures (Table A1).

The FAC means for each basin are shown for both models in Table 1. The central west has the highest basin-mean FAC in both SNOWPACK (24.8±4.6 m) and the CFM (19.5±3.7 m). In both models, the southeast and northwest have similarly high basin-mean FAC values. The lowest basin-mean FAC occurs in the southwest in SNOWPACK (17.4±7.6 m) and the CFM (13.9±5.8 m). The best model agreement is in the northeast and north basins where the difference is 13 % and 15 %, respectively (Table 1). The spatially-integrated FAC is the total air volume within the firn layer and is shown in Table 2 averaged for the first (1980) and last (1995) years of the RCI for each basin. We compare these two years to confirm that no change in FAC occurs between the start and end of the RCI that is used for the spin-up. In both SNOWPACK and the CFM, all basins experience less than a 1 % change between the two years, which verifies the steady-state assumption of the RCI and the design of the spin-up (Table 2).

We examine temporal patterns in FAC spatially integrated across the full ice sheet (Fig. 8) and over each basin (Fig. 9). During the 1980–1995 RCI, there is no strong trend in the full ice sheet's air content in either model (Fig. 8), which is consistent with our assignment of that time period as the RCI. By design of the spin-up, there are no substantial changes in the spatially-integrated FAC between the start and end of the RCI, which means the change to Greenland's sea level rise buffering capacity is also negligible. Both SNOWPACK and the CFM simulate a short-term increase in FAC from 1982 until 1987, followed by a decrease in FAC until 1990 (Fig. 8). Patterns of short-term (∼1–5 years) variability are more prevalent in each basin (Fig. 9). The same increasing then decreasing pattern in Fig. 8 is evident in the basin-averaged FAC in the northeast and southeast, and somewhat detectable in other basins (Fig. 9). Only in the north basin are the short-term trends absent.

To examine how the models represent the seasonal cycle in spatially-integrated FAC, we remove the annual means and then fit a sine wave to the data (Fig. A3). We quantify a seasonal "breathing" signal from the amplitude following methods from Ligtenberg et al. (2012). The amplitudes of the seasonal signals in the spatially-integrated FAC for each basin are reported in Table 3. In SNOWPACK, the strongest signal during the RCI is in the southeast, and the weakest is in the northeast. In the CFM, the strongest signal is also in the southeast, whereas the weakest is in the north where the seasonality was undetectable by the chosen methods. Integrated across the full ice sheet, the seasonal signal is about two times greater in the CFM (129 km^3) compared to SNOWPACK (61 km^3) (Table 3; Figs. 8, A3).

https://doi.org/10.5194/tc-2022-223
Preprint. Discussion started: 1 December 2022

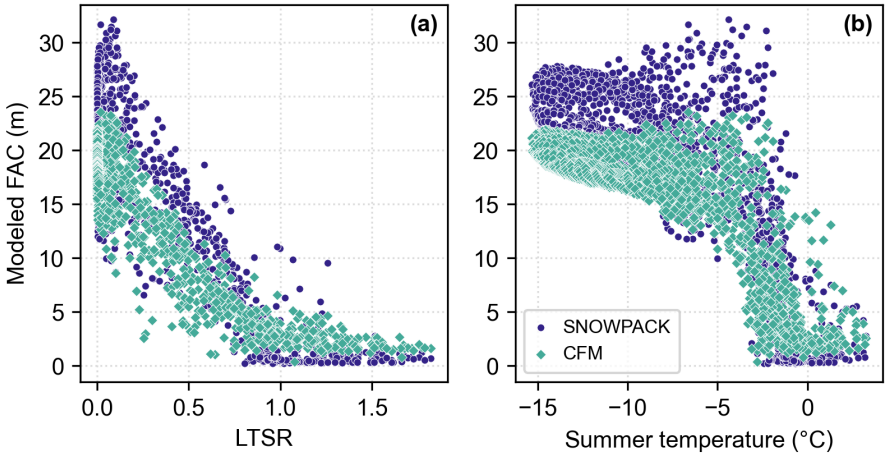

Figure 5. Modeled firn air content (FAC) in SNOWPACK (blue) and the CFM (green) as a function of (a) the liquid-to-solid ratio (LTSR, Eq. 6), and (b) the summer 2-m air temperature all calculated for 1980 through 1995.

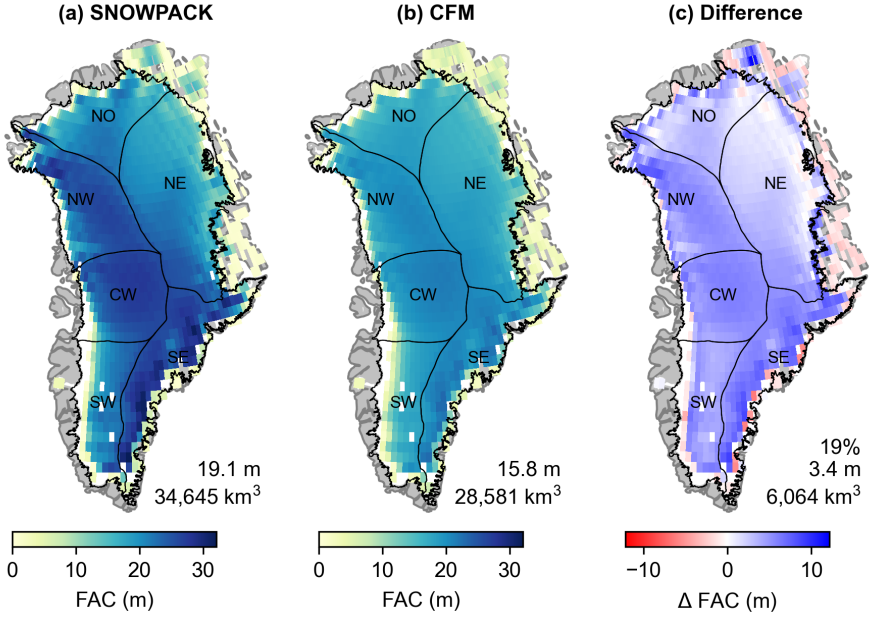

Figure 6. Modeled reference climate interval (RCI, 1980–1995) mean firn air content (FAC) calculated over the upper 100 m of the firn column from (a) SNOWPACK and (b) the CFM. (c) SNOWPACK minus the CFM calculated FAC. The values in the bottom right of each panel are the mean FAC and spatially-integrated FAC. Panel (c) also includes the percent difference. Areas where one or both of the models having missing data are shown in white. Black outlines show the six basins defined by Rignot and Mouginot (2012).

https://doi.org/10.5194/tc-2022-223
Preprint. Discussion started: 1 December 2022

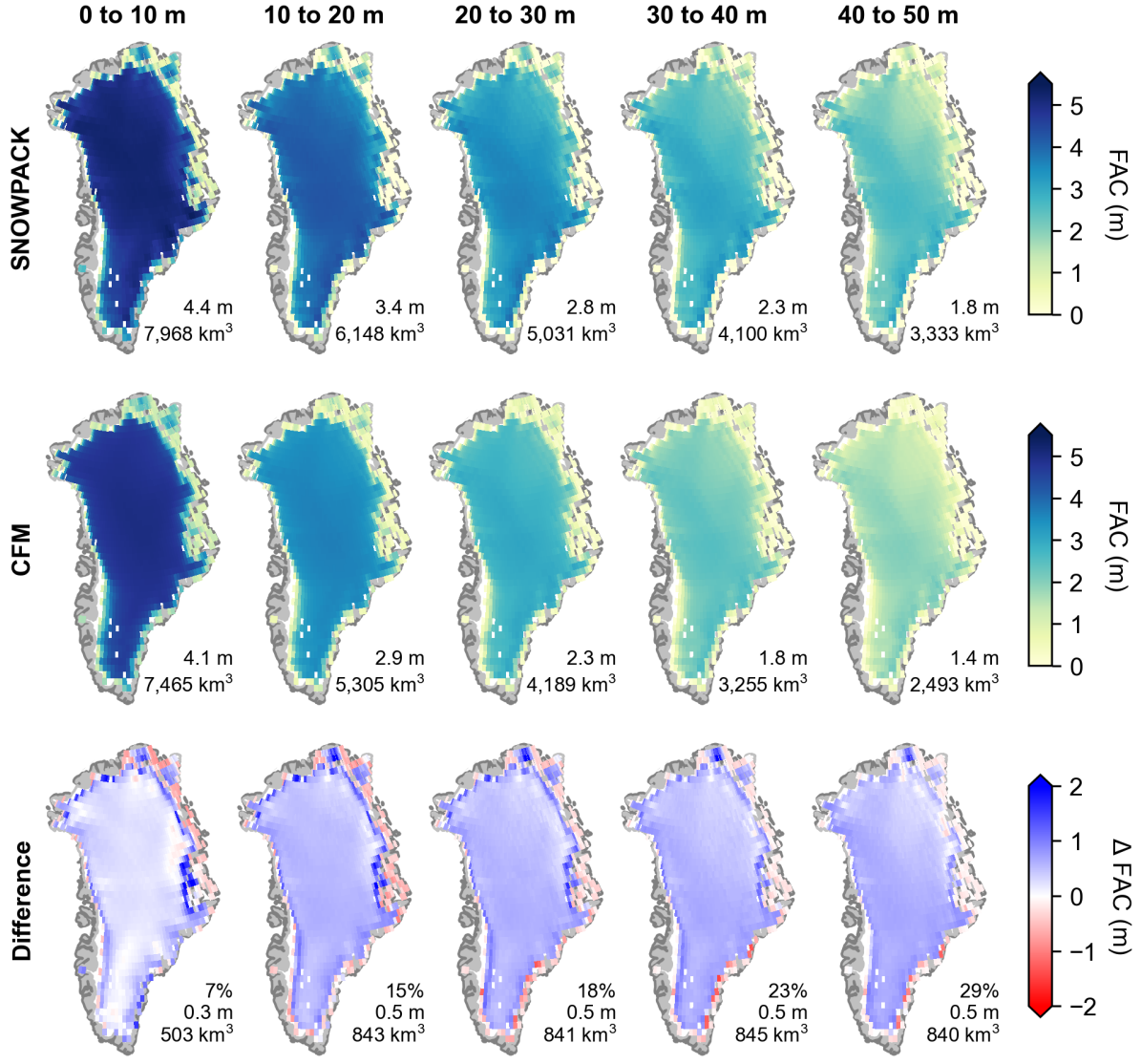

Figure 7. Modeled reference climate interval (RCI, 1980–1995) mean firn air content (FAC) calculated for 10-m-thick vertical segments over the GrIS. Top row: SNOWPACK, middle row: the CFM, bottom row: SNOWPACK minus the CFM. The values in the bottom right of each panel are the mean FAC and spatially-integrated FAC. The bottom row also includes the percent difference.

https://doi.org/10.5194/tc-2022-223
Preprint. Discussion started: 1 December 2022

The Cryosphere Discussions
Open Access
EGU

Table 1. Mean modeled firn air content (FAC) for the 1980–1995 reference climate interval (RCI) and for the 2005–2020 period, averaged across each of the six basins shown in Fig. 6. FAC is reported as mean±standard deviation, and the percent difference between SNOWPACK and the CFM is also shown. The last row shows the statistics for all basins together.

	1980–1995			2005–2020		
Basin	CFM FAC (m)	SNOWPACK FAC (m)	% difference	CFM FAC (m)	SNOWPACK FAC (m)	% difference
NW	18.5±4.1	23.3±5.2	23	18.5±4.4	23.1±5.8	22
CW	19.5±3.7	24.8±4.6	24	19.8±4.0	24.8±5.2	22
SW	13.9±5.8	17.4±7.6	23	13.7±6.1	16.9±8.0	21
NO	15.5±4.6	18.1±5.1	15	15.2±4.8	17.5±5.5	14
NE	16.6±3.5	19.0±4.4	13	16.5±3.8	18.7±4.8	13
SE	18.8±4.8	23.7±7.7	23	18.8±5.1	23.4±7.9	22
All	15.8±6.0	19.1±8.0	19	15.7±6.3	18.8±8.4	18

Table 2. Modeled spatially-integrated firn air content (FAC) for each of the six basins (Fig. 6) at the beginning and end of the 1980–1995 reference climate interval (RCI) and the 2005–2020 period. The percent change between 1980 and 1995, and 2005 and 2020 is reported for each model. The last row shows the statistics for all basins summed together.

	CFM			SNOWPACK			CFM			SNOWPACK		
	1980	1995	%	1980	1995	%	2005	2020	%	2005	2020	%
Basin	(km^3)	(km^3)	change	(km^3)	(km^3)	change	(km^3)	(km^3)	change	(km^3)	(km^3)	change
NW	4977	4953	-0.5	6279	6256	-0.4	5015	4937	-1.5	6322	6114	-3.3
CW	4254	4241	-0.3	5392	5390	-0.0	4323	4264	-1.4	5476	5301	-3.2
SW	2332	2328	-0.1	2911	2915	+0.1	2380	2250	-5.4	2992	2745	-8.3
NO	3482	3483	+0.0	4046	4049	+0.1	3435	3351	-2.5	3992	3830	-4.1
NE	7961	7968	+0.1	9069	9081	+0.1	7894	7906	+0.2	9012	8961	-0.6
SE	4739	4722	-0.4	5946	5928	-0.3	4745	4737	-0.2	5989	5879	-1.8
All	27745	27695	-0.2	33643	33619	-0.1	27792	27445	-1.2	33783	32830	-2.8

https://doi.org/10.5194/tc-2022-223
Preprint. Discussion started: 1 December 2022

The Cryosphere Discussions

Table 3. The seasonal breathing signal in each of the six basins (Fig. 6) for the 1980–1995 reference climate interval (RCI) and the 2005–2020 period. The seasonal signal is the amplitude of the best fit sine curve to the the spatially-integrated FAC anomalies (Fig. A3). Undetectable signals are reported as "N/A", and the last row shows the values for all basins together.

	1980–1995		2005–2020	
Basin	CFM signal (km^3)	SNOWPACK signal (km^3)	CFM signal (km^3)	SNOWPACK signal (km^3)
NW	4	9	8	N/A
CW	5	6	9	4
SW	17	5	23	13
NO	N/A	5	4	N/A
NE	11	4	15	N/A
SE	49	25	53	33
All	129	61	165	117

3.3 Firn properties in a changing climate

We now turn our attention to a period where the GrIS was undergoing realtively more change. In the 2005–2020 period, the ice-sheet-wide mean FAC is slightly less than that of the 1980–1995 period for both models, but the difference is not statistically significant (p = 0.08 for SNOWPACK, p = 0.30 for the CFM) (Table 1). Between the two periods, the basin-averaged FAC values are not statistically different (p > 0.05 in all basins). In both models, the highest basin-averaged FAC is still in the central west, and the lowest is still in the southwest. Additionally, the best model agreement (13 % difference) still occurs in the northeast (Table 1).

After the 1980–1995 RCI, trends in spatially-averaged FAC begin to emerge in the full ice sheet signal (Fig. 8). SNOWPACK models a decreasing trend of -66.6 km^3 yr^{-1} during the 2005–2020 period, which is significantly greater in magnitude than the trend of 1.7 km^3 yr^{-1} throughout the RCI (p < 0.05). A consistent decreasing trend is modeled from ∼2002 and through ∼2011. Two extreme FAC depletion events are captured in 2012 and 2019 (Fig. 8a). Between 1980 and 2020, SNOWPACK simulates a loss of 1043 km^3 of firn pore space, which could store liquid water equivalent to 2.9 mm of sea level rise. The pattern is similar but dampened in the CFM record (Fig. 8b). The 2005–2020 trend of -17.4 km^3 yr^{-1} is less than that of SNOWPACK (p < 0.05) but is still statistically different from the RCI trend of (p < 0.05). The CFM shows less depletion of FAC, with only 356 km^3 of pore space lost (1.0 mm sea level rise) by the end of 2020 compared to 1980.

Similarities and differences in short-term trends are modeled across each basin (Fig. 9). In the north and northeast, both models show that FAC generally decreases with time and is lower in the more recent 2005–2020 period compared to the reference climate interval, consistent with FAC depletion due to increased melt and associated water percolation processes. The interannual variability is strongest in the southeast where there is no clear increasing or decreasing trend following the RCI. In the southwest, FAC is fairly constant until it rapidly drops in 2012. Following this, FAC continues to show no clear

https://doi.org/10.5194/tc-2022-223
Preprint. Discussion started: 1 December 2022

trend. The northwest and central west show similar patterns in FAC with values increasing from 1995 to until 2005. After 2005, SNOWPACK FAC decreases while the CFM FAC remains relatively constant (Fig. 9).

With the exceptions of the northwest and central west, SNOWPACK and the CFM generally simulate the same trends in FAC (Fig. 9). However, in all cases, differences arise in seasonal variability and magnitudes of change. In all basins, the two models begin to diverge between 2005 and 2012. SNOWPACK simulates greater negative changes in FAC compared to the CFM once the models diverge. In most basins, both models capture an extreme drop in FAC in 2012 associated with the extreme melt occurring in that year, followed by an increase in FAC in the northeast and southeast. The rapid depletion is greatest in the southwest but less pronounced in the central west and north basins. The magnitude of the 2012 depletion is similar in SNOWPACK and the CFM (Fig. 9).

The seasonal breathing signal is stronger in the CFM (165 km^3) compared to SNOWPACK (117 km^3) in the 2005–2020 period (Table 3; Fig. A3). In both models, the southeast basin has the strongest seasonality. The weakest signal in the CFM is in the north, and in SNOWPACK the signal is too weak to be detected in the northwest, northeast, and north basins. Additionally, the amplitude of the seasonal signal is greater in the 2005–2020 period compared to the 1980–1995 RCI for most basins and for the full ice sheet (Table 3; Fig. A3).

In the 2005 to 2020 period, both models simulate a decrease in FAC, especially in many of the marginal areas of the ice sheet (Fig. 10). The spatially-integrated FAC across the full ice sheet decreases by 953 km^3 in SNOWPACK, and by 347 km^3 in the CFM (Table 2). Both SNOWPACK and the CFM show substantial FAC loss in the western basins. In SNOWPACK, the southwest basin's spatially-integrated FAC decreases by 248 km^3, which is a -8.3 % change. In the CFM, there is a decrease in the southwest basin of 129 km^3, which is a -5.4 % change. The models simulate increasing FAC in some parts of the eastern basins, leading to small percent changes in the northeast and southeast. In fact, the only instance of a positive net change is the 0.2 % increase simulated by the CFM in the northeast basin (Table 2). Individual grid cells showing positive change in FAC during this period are mostly in the northeast and southeast basins (Fig. 10).

Observations have shown that FAC is not completely indicative of available pore space to store meltwater when thick near-surface ice slabs are present in the firn. To evaluate how both firn models reproduce the formation of near-surface ice layers, we identify which grid cells simulate ice slabs in the top 20 m of the ice column in April 2014. We choose this depth and date in order to directly compare to ice slabs detected by IceBridge accumulation radar (MacFerrin et al., 2019). We define an ice slab as a layer with a density of at least 830 kg m^{-3} and a thickness of at least 1 m. Our algorithm outputs the depth and thickness of the ice slab nearest to the surface, which in some cases could be bare ice at the surface since there is no condition that the ice slab must be beneath a layer of snow or firn. The distribution of modeled ice slabs is largely constrained to the marginal regions of the ice sheet (Fig. 11). Both SNOWPACK and the CFM simulate high concentrations of ice slabs in the margins and ablation zone. Most of the ice slabs detected by IceBridge accumulation radar in 2014 (MacFerrin et al., 2019) overlap with the simulated ice slabs. SNOWPACK simulates ice slabs in 459 grid points, and the mean depth of those slabs is 2.49 m. The CFM simulates ice slabs in 369 grid points, and the mean depth to those slabs is 3.81 m.

https://doi.org/10.5194/tc-2022-223
Preprint. Discussion started: 1 December 2022

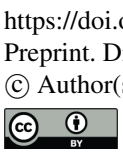

The Cryosphere
Discussions
Open Access
EGU

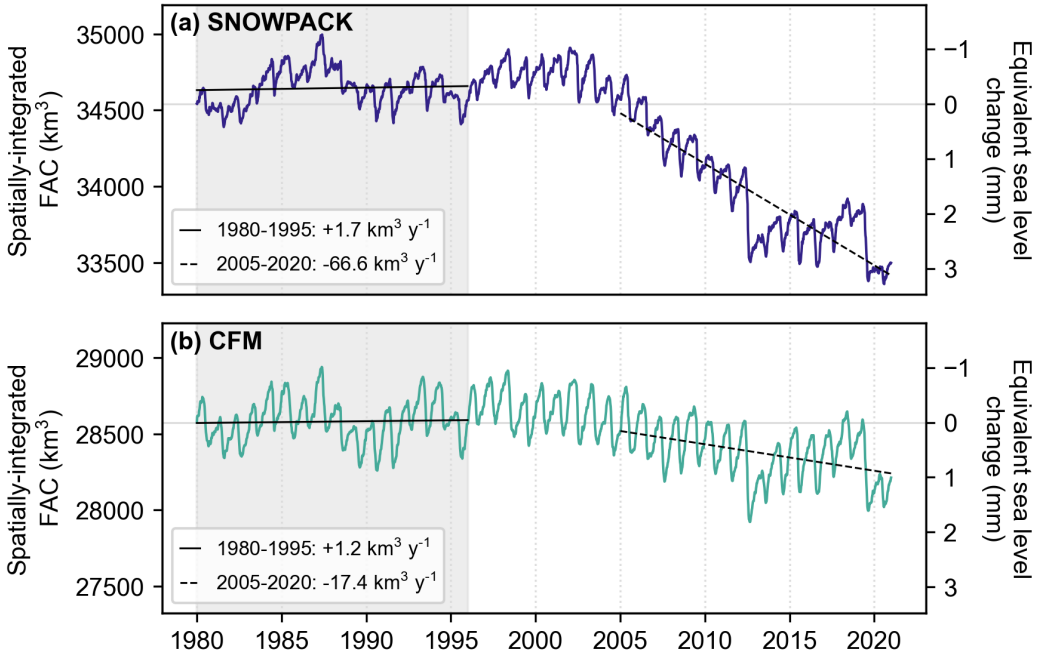

Figure 8. Weekly firn air content (FAC) spatially-integrated across the full ice sheet from (a) SNOWPACK and (b) the CFM. The left y-axis shows the FAC, and the right y-axis shows the equivalent change in sea level buffering capacity relative to 1980. The gray shading represents the 1980–1995 reference climate interval (RCI). The solid black lines are the trends in spatially-integrated FAC for 1980–1995, and the dashed lines are the trends for 2005–2020.

4 Discussion

4.1 Model evaluation

Both firn models perform equally well, and their high NSE coefficients ($\geq$0.90) and low errors (MAPEs $\leq$16 %) demonstrate their generally good agreement with observed FAC from the SUMup dataset. The nature of the discrepancies between the modeled and observed properties tend to differ between the two models. The +7.9 % relative bias in SNOWPACK FAC demonstrates that the model tends to overestimate FAC. This bias in SNOWPACK has been shown in both Greenland (Steger et al., 2017) and Antarctica (Keenan et al., 2021). However, Keenan et al. (2021) also showed that SNOWPACK outperformed other semi-empirical models in the uppermost 10 m in locations where the models were uncalibrated to the observations, which underscores the utility of SNOWPACK in locations where observations of firn properties are sparse or rapidly changing. In contrast, the CFM tends to produce smaller FAC values and has a smaller bias of +0.2 %. The signature of model biases differs across the ice sheet as climate, topography, and the impact of firn hydrology vary. Below we explore the highest model biases and consider the conditions that cause SNOWPACK and the CFM to differ from each other and from the observations.

https://doi.org/10.5194/tc-2022-223
Preprint. Discussion started: 1 December 2022

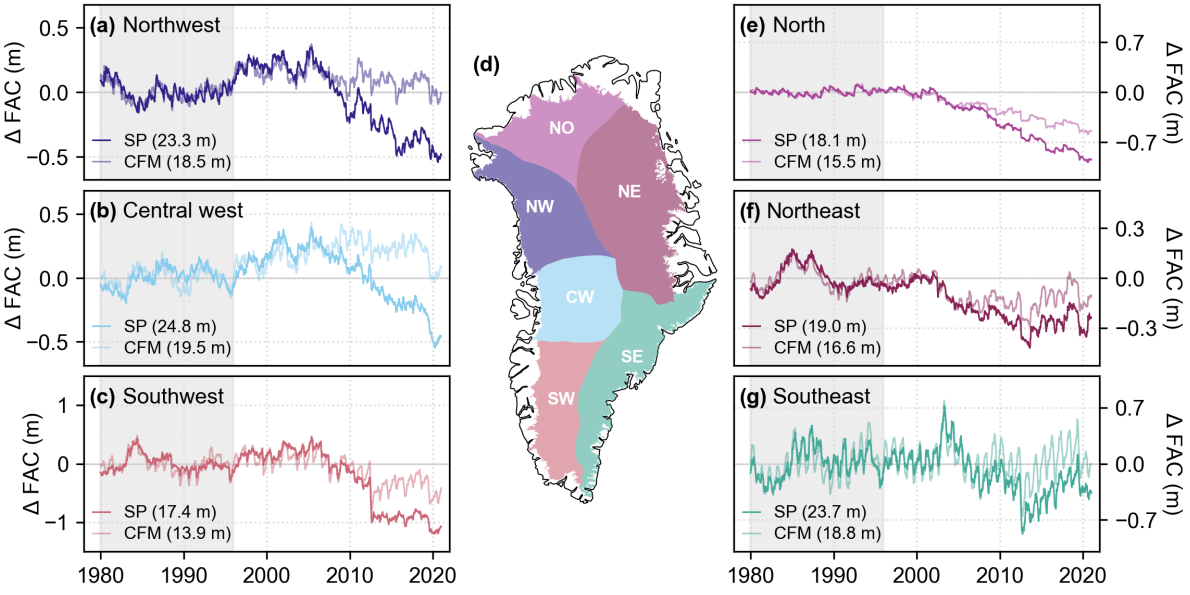

Figure 9. (a-c, e-g) Time series of the basin-averaged weekly firn air content (FAC) anomaly from the reference climate interval (RCI, 1980–1995; gray shading) mean, which is shown in the bottom left of each panel. Results from SNOWPACK are shown as the darker lines and the results from the CFM are shown as the lighter lines. (d) Greenland's six basins defined by Rignot and Mouginot (2012) used for calculating trends in firn air content (FAC).

Some of the highest model biases in SNOWPACK and the CFM occur in southeast Greenland and are likely a result of two factors. First, the observed density profiles are from cores that were drilled directly into a perennial firn aquifer (Miller et al., 2018). These particular cores approach bulk densities of 1000 kg m^{-3} due to the liquid water contained within the pore space of the firn. Neither model captures the high densities resulting from the firn aquifer because the use of bucket scheme in the models prevents full saturation in the firn. A firn hydrology model intercomparison study that included outputs from the CFM (but not SNOWPACK) found that none of the nine models included accurately simulated meltwater infiltration at the four study sites (Vandecrux et al., 2020a). Moreover, Steger et al. (2017) found that the largest model differences between SNOWPACK and IMAU-FDM (a semi-empirical firn model) occur in the southeast margin of the ice sheet where firn aquifers form. Our results agree with these findings that model differences are highest where liquid water is present, indicating that poor representation of meltwater percolation processes is still a substantial limiting factor in firn model performance.

An additional reason why the model bias is high in the southeast is likely the coarseness of the forcing grid in relation to the steep ice sheet topography in this area. The observed cores in Figure 4 are all closest to the same MERRA-2 grid point and therefore all have the same atmospheric forcing. However, the cores are located along a transect that spans a steep elevation gradient. Within these five cores, the lowest relative bias occurs at the point that is closest to the MERRA-2 grid point center (i.e., furthest west along the transect) and where the elevation is highest (Fig. 4c). The highest relative bias occurs at the

https://doi.org/10.5194/tc-2022-223
Preprint. Discussion started: 1 December 2022

The Cryosphere Discussions
Open Access
EGU

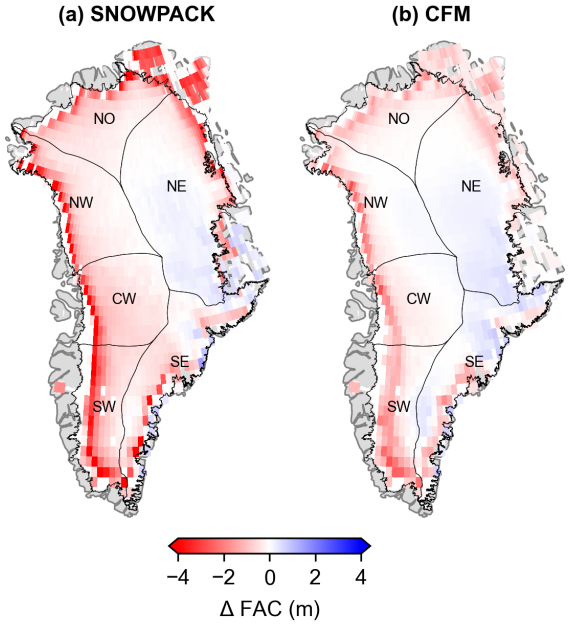

Figure 10. Modeled difference in mean firn air content (FAC) between 2005 and 2020 for (a) SNOWPACK and (b) the CFM. Black outlines show the six basins defined by Rignot and Mouginot (2012).

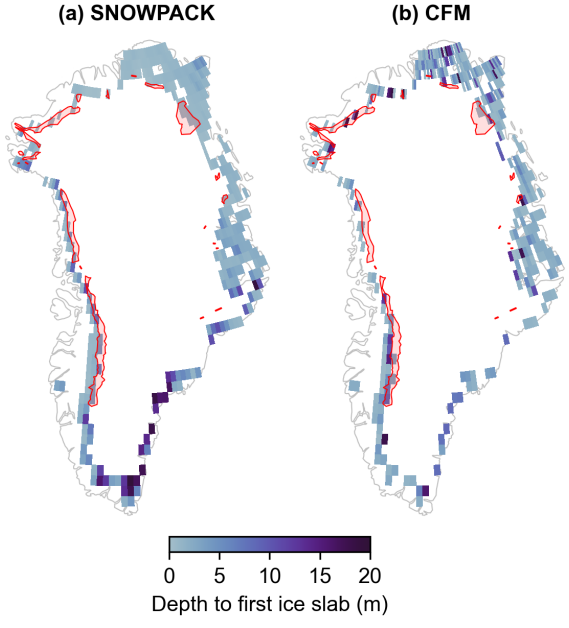

Figure 11. Modeled and observed ice slabs in 2014. Red polygons show ice slabs detected by IceBridge accumulation radar (MacFerrin et al., 2019). Modeled ice slabs are shaded by the depth to the first ice layer that is at least 1 m thick.

https://doi.org/10.5194/tc-2022-223
Preprint. Discussion started: 1 December 2022

point furthest from the MERRA-2 grid point, where the elevation is lowest, and where the observed vs. MERRA-2 elevation difference is greatest (Fig. 4g). The steep topography may also lead to strong spatial variations in atmospheric processes such as orographic precipitation, which is not well represented on such a coarse grid (van Kampenhout et al., 2019). This demonstrates the limitations of a coarsely-gridded forcing, especially in steeply sloped areas where climate is likely to be highly variable within a single grid cell.

Despite the few instances of relatively high disagreement between the models and observations, the overall good performance of both models in simulating observations gives confidence in the models' abilities to simulate firn properties across the full ice sheet. Model uncertainty in areas with firn aquifers or steep surface topography is likely to be higher compared to results from flatter, dry firn zones in the ice-sheet interior.

4.2 Firn air content response to atmospheric forcing

Since we use identical atmospheric data to force the models, differences in the modeled firn properties are purely due to differences in the models themselves. The models are particularly distinct in their response to the LTSR and summer air temperature (Fig. 5). Both models show an inverse, non-linear response between LTSR and FAC (Fig. 5a). However, there is more spread in SNOWPACK FAC compared to the CFM FAC, especially for low values of LTSR where snowfall is a larger contributor to surface input. Because there is less spread in the CFM FAC, the LTSR is a stronger predictor of FAC in the CFM compared to SNOWPACK. The large range of possible SNOWPACK-simulated FAC values at low LTSR values is likely due to the model's sophisticated new-snow density scheme that uses more than only air temperature and accumulation to determine near-surface density. In the presence of more liquid surface input (i.e., when the LTSR is high), SNOWPACK produces consistently lower FAC values compared to the CFM. This indicates that when more liquid water is present compared to snowfall, the CFM still simulates available pore space while SNOWPACK's FAC is near-zero in most cases. The response of FAC to the LTSR is important in our consideration of future climate change since we may see the LTSR increase with future warming. In a transition from lower to higher LTSR values, and by proxy, in a transition to a warmer and wetter climate, the CFM shows a more gradual decline in FAC and SNOWPACK shows a more pronounced drop toward near-zero FAC values. These responses to the LTSR can be seen in western Greenland where the CFM FAC gradually decreases moving from the interior to the ice sheet margin (Fig. 6b), and SNOWPACK FAC sharply drops off in the same area (Fig. 6a). This is an area vulnerable to climate change where increased ice slab formation and decreased firn storage capacity has already been detected (de la Peña et al., 2015).

Additionally, we examine the summer air temperature since it can be directly derived from climate model output unlike the LTSR, which requires more detailed output from a dedicated firn model. We find that a temperature threshold appears to control FAC; at ∼-4°C, FAC in both models rapidly drops (Fig. 5b). The greatest range in FAC and the highest FAC values occur near this temperature for SNOWPACK and the CFM. Between ∼-4 and ∼0°C, the models simulate almost the full range of FAC. Therefore, outside of the -4–0°C window, temperature is a relative good predictor of FAC, especially in the CFM where the spread in FAC is less than in SNOWPACK. In both summer air temperature and the LTSR, the spread in the SNOWPACK values shows that FAC is more than just a function of a single variable or metric, and it points to the complexity

https://doi.org/10.5194/tc-2022-223
Preprint. Discussion started: 1 December 2022


The Cryosphere Discussions

of the model. Generally, the FAC simulated by the CFM is easier to predict using LTSR or summer temperature when compared to SNOWPACK.

4.3 Spatial and temporal patterns in firn air content

To place our results in the context of other firn studies, we explore how the modeled FAC compares to existing estimations. We note that this is not a direct comparison since choices of atmospheric forcing, model domain boundaries, and temporal periods will generate differences in FAC that are independent from the firn model choice. Still, we use this comparison to validate the order of magnitude of our results. Our modeled FAC integrated across the full ice sheet for the upper 100 m from the CFM (28,581 km^3) is very similar to a 2010–2017 value (26,800 km^3) calculated from observations (Vandecrux et al., 2019). SNOWPACK's FAC of 34,645 km^3 is on the same order but still larger than the observations and the CFM-modeled value. SNOWPACK's spatially-integrated FAC in the upper 100 m is close to a regional climate model's (HIRHAM5_MOD) estimate for this period (Vandecrux et al., 2019).

SNOWPACK and the CFM simulate reasonable ice-sheet-wide FAC when compared to other studies, but the two models still differ in magnitude (Fig. 6). In the upper 10 m, the models agree within ± 10 %. However, with increasing depth, the model agreement worsens (Fig. 7). This suggests that the difference in spatially-integrated FAC between the two models arises from the differences in densification with depth. SNOWPACK uses the constitutive relationship between stress and strain in snow to calculate firn densification, while the CFM's densification rate is determined using a semi-empirical equation tuned with firn depth-density data. The higher FAC at greater depths predicted by SNOWPACK indicates that its modeled densification rate is slower in the deeper firn than the rate in the CFM. This could be related to the fact that SNOWPACK was developed using data from seasonal alpine snow which may not be representative of the physical processes driving deep firn densifcation. Similarly, Stevens et al. (2020) found that the physically-based snow model Crocus predicted slower densification at Summit, Greenland than other firn densification equations. Determining which model performs better at depth (and by proxy, whether the physics-based or empirical approach is recommended) is hindered by the paucity of deep firn observations that could provide insight into densification processes.

Further differences in SNOWPACK and the CFM are seen in the modeled time series of FAC. Both models show a substantial depletion of FAC from 2005 through 2020, but the CFM's response is smaller than that of SNOWPACK. During this time, SNOWPACK's simulated trend of -66.6 $km^3\ yr^{-1}$ corresponds with a -2.8 % change in spatially-integrated FAC. The CFM's simulated trend of -17.4 $km^3\ yr^{-1}$ is smaller and the change is also less at -1.2 %. While the magnitudes of trends and FAC changes are greater in SNOWPACK, seasonal signals are greater in the CFM. The stronger seasonality in the CFM is indicative of the model's more simple treatment of forcing data like accumulation and temperature, which have strong seasonal patterns. SNOWPACK's same sophisticated new-snow density scheme that leads to a complex relationship between LTSR and FAC also results in this smaller seasonal signal.

Partitioning the record of FAC into climatologically distinct basins reveals further differences in the models and spatial variability. Notably, the signature of the 2012 extreme melt season can be seen as an abrupt drop in FAC in most basins (Fig. 9). In the southeast, northeast, and northwest, both models show that FAC begins to rebound immediately after the 2012

https://doi.org/10.5194/tc-2022-223
Preprint. Discussion started: 1 December 2022

depletion. This replenishing of the firn pore space has also been observed in shallow firn cores following the extreme 2012 melt season (Rennermalm et al., 2021). In the southwest, this rebound is only detected in the CFM and not SNOWPACK, which again demonstrates some of the discrepancies between the models. Still, both models generally capture the ice sheet's rebuilding of some of the porous firn layer lost during an extreme melt event.

While spatially-integrated FAC describes the total volume of pore space in the GrIS, permeability and access to pore space is important for fully understanding the buffering capacity. Ice slabs, which render deep pore space inaccessible to meltwater (Machguth et al., 2016), are simulated in the ice sheet's marginal areas where the highest FAC depletion occurs between 2005 and 2020. In fact, the largest percent change is in the southwest, has the warmest temperatures and highest melt compared to other basins during this period (Table A2). These findings agree well with observations that reveal significant FAC depletion in the low-accumulation percolation zone in western Greenland related to increased melt (Vandecrux et al., 2019). Pore space depletion can also be a sign of firn densification, which has been found to increase cold content in the firn and amplify meltwater freezing and ice slab formation in the near-surface (Vandecrux et al., 2020a). FAC depletion is found where ice slabs are simulated, and up-glacier from these ice slabs (Figs. 10, 11). This FAC depletion and firn densification may prime the firn for future migration of ice slabs toward the ice-sheet interior. The differences in the modeled ice slab locations and depths is likely attributed to the overall diverging behavior of the models in wet firn zones, which agrees with findings in the RetMIP firn model intercomparison study (Vandecrux et al., 2020b).

5 Conclusions

An evaluation of the physics-based firn model SNOWPACK, and the semi-empirical CFM reveals overall high model performance when compared with observations from the SUMup dataset. The Nash-Sutcliffe efficiency (NSE) coefficient for SNOWPACK is 0.90 and for the CFM is 0.94, and the mean average percentage error (MAPE) is 14 % for SNOWPACK and 16 % for the CFM. The highest model biases occur in the marginal areas of the ice sheet, which is where conditions for predicting FAC (e.g., melt, snowfall, topography) are most variable. Comprehensive model evaluation is hindered by the shortage of deep firn observations and the spatial coverage of observations. Still, the overall success of the models and understanding of their limitations allow us to perform full ice sheet simulations and place our results in a context of uncertainty.

The use of identical atmospheric forcing lets us isolate the differences in the models themselves and examine how they respond to the same forcing. The summer air temperature acts as a metric for examining the impact of forcing conditions on FAC, and reveals high model agreement in warmer temperatures where FAC abruptly decreases above a threshold temperature of ∼-4°C. We also employ the liquid-to-solid ratio (LTSR) as a metric summarizing the climatological regime of accumulation and melt. While FAC in the CFM more gradually decreases as the LTSR increases, SNOWPACK FAC decreases more rapidly and reaches near-zero FAC values that the CFM does not capture. These different responses in air content to increasing liquid water will become important in future warming scenarios and we expect the models to diverge even more. As such, further work is needed to improve our understanding of the physics of firn hydrology, which will consequently improve the ability

https://doi.org/10.5194/tc-2022-223
Preprint. Discussion started: 1 December 2022

of models to simulate FAC response to increased melt and liquid water. This will in turn allow us to better predict the firn's response to future warming.

The spatially-integrated FAC during the 1980–1995 RCI is 34,645 km^3 from SNOWPACK and 28,581 km^3 from the CFM, which are both reasonable estimations when compared to other studies, though the inconsistencies in atmospheric forcing data, model domain area, and temporal periods render comparisons between studies difficult. Our spin-up is designed such that no significant change occurs in FAC between the start and end of the 16-year period. However, in a more recent period of the same length (2005–2020), substantial loss of pore space is modeled as a -2.8 % change in SNOWPACK and -1.2 % change in the CFM. The highest loss of pore space occurs in the ice sheet's western margins where near-surface ice slabs are detected both by the models and observations. This highlights the vulnerability of the firn layer's meltwater storage capacity, especially in these low-elevation and high-melt areas. Notably, the pore space depletion is more extreme in SNOWPACK. It simulates a larger magnitude of change and a more negative 2005–2020 trend (-66.6 $km^3\ yr^{-1}$) compared to the CFM (-17.4 $km^3\ yr^{-1}$). Over the full 41-year period, SNOWPACK simulates a loss of pore space equivalent to storing 3 mm of sea level rise, while the CFM firn loses only 1 mm. Although these longer-term changes are greater in SNOWPACK, the strength of the seasonal signal in the CFM is much greater, again pointing to the different treatment of atmospheric input to the models and the differing complexities of the models.

https://doi.org/10.5194/tc-2022-223
Preprint. Discussion started: 1 December 2022

The Cryosphere Discussions
Open Access
EGU

Appendix A

Table A1. Mean atmospheric forcing variables for the 1980–1995 reference climate interval (RCI), averaged across each of the six basins shown in Fig. 6. Values are reported as mean±standard deviation.

Basin	Temperature (°C)	Precip. (mm w.e. yr^{-1})	RH (%)	Wind (m s^{-1})	ISWR (W m^{-2})	ILWR (W m^{-2})	Melt (mm w.e. yr^{-1})
NW	-23.5±4.8	390.5±204.4	92.2±5.5	4.6±1.2	115.8±6.7	169.8±15.6	43.1±117.2
CW	-23.4±4.0	427.3±132.0	92.6±4.8	5.7±1.4	127.2±4.0	171.9±12.1	31.5±103.0
SW	-17.0±3.7	659.9±368.4	87.1±5.3	7.9±1.7	138.4±7.8	191.1±12.8	255.2±345.6
NO	-24.3±3.2	192.5±63.0	91.5±4.8	3.9±0.9	111.0±5.3	164.2±10.2	23.7±61.6
NE	-25.4±4.2	188.0±89.0	90.1±7.7	4.0±1.7	122.7±5.9	158.6±11.6	15.9±50.6
SE	-16.8±5.6	1049.4±681.3	85.4±7.2	6.0±2.5	132.6±7.4	191.4±20.2	262.5±427.4

Table A2. Mean atmospheric forcing variables for the 2005–2020 period, averaged across each of the six basins shown in Fig. 6. Values are reported as mean±standard deviation.

Basin	Temperature (°C)	Precip. (mm w.e. yr^{-1})	RH (%)	Wind (m s^{-1})	ISWR (W m^{-2})	ILWR (W m^{-2})	Melt (mm w.e. yr^{-1})
NW	-22.1±4.7	399.1±212.3	91.5±6.2	4.7±1.3	116.8±6.8	173.8±14.9	78.2±184.2
CW	-22.0±4.1	427.7±137.3	92.1±5.1	5.8±1.5	128.2±4.1	176.4±12.5	58.0±166.2
SW	-15.5±3.6	641.5±363.3	86.9±5.4	7.7±1.6	138.7±7.6	196.3±13.0	353.3±426.4
NO	-22.8±3.2	164.1±46.2	90.5±5.9	3.7±0.9	113.5±4.8	167.2±9.5	48.0±104.6
NE	-24.0±4.3	190.5±95.3	89.6±8.3	3.9±1.8	124.0±5.6	162.8±11.6	29.8±81.3
SE	-15.7±5.6	1079.2±745.9	85.1±7.8	6.0±2.6	133.0±7.2	195.9±20.5	313.3±477.6

https://doi.org/10.5194/tc-2022-223
Preprint. Discussion started: 1 December 2022

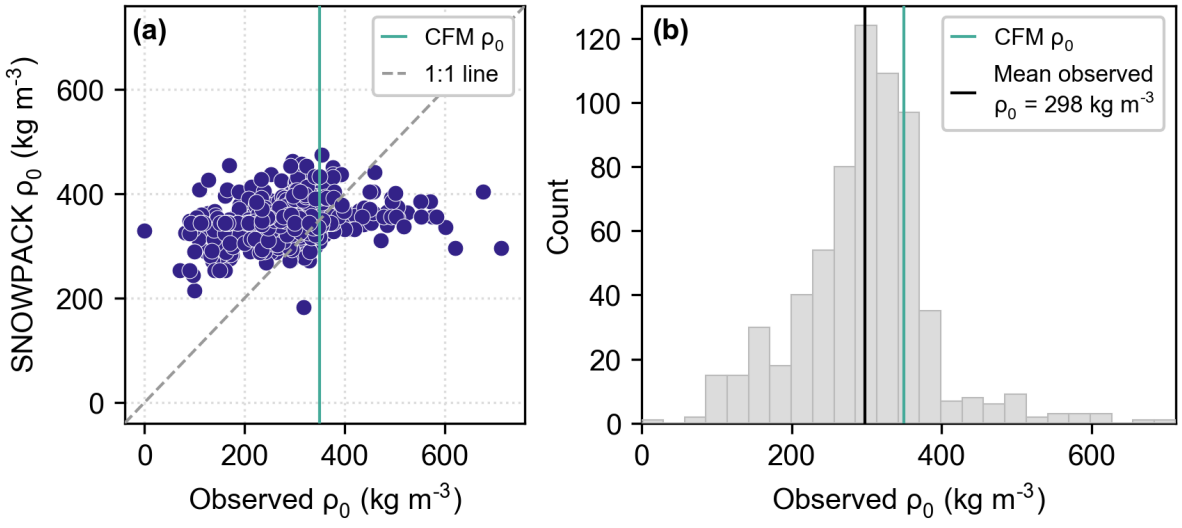

Figure A1. (a) Observed surface density (ρ_0) from SUMup versus SNOWPACK. Since some observations begin farther below the surface, observed ρ_0 is defined as the uppermost density measurement that is within 0.1 m from the surface. The SNOWPACK ρ_0 is calculated over the same vertical segment as the SUMup observation. The CFM uses a prescribed surface density of 350 kg m^{-3}, which falls near many of the observed surface densities (green vertical line). (b) Histogram of observed surface density with the mean represented by the black line. Also plotted is the CFM surface density of 350 kg m^{-3}.

https://doi.org/10.5194/tc-2022-223
Preprint. Discussion started: 1 December 2022

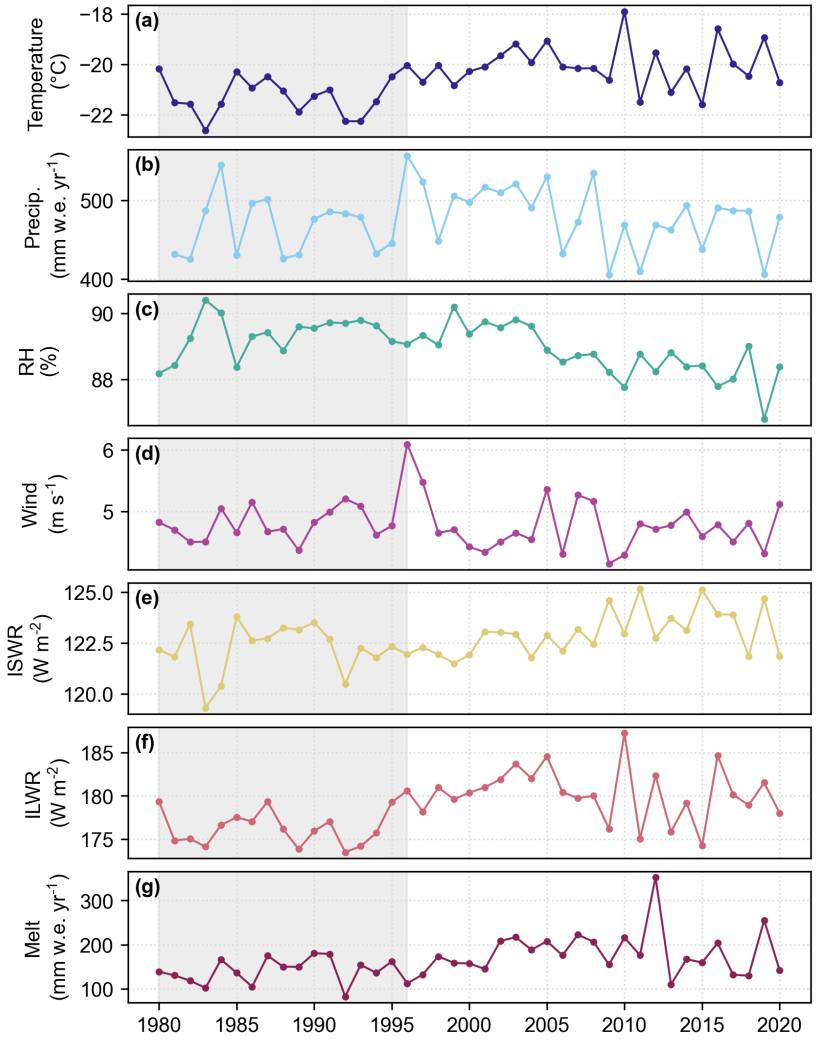

Figure A2. Time series of annually-averaged MERRA-2 forcing variables: (a) temperature, (b) precipitation, (c) relative humidity, (d) wind, (e) incoming shortwave radiation (ISWR), and (f) incoming longwave radiation (ILWR) averaged across the full ice sheet. Also shown is (g) the annually-summed melt output from SNOWPACK used as forcing in the CFM. Gray shading represents the reference climate interval from 1980 to 1995.

https://doi.org/10.5194/tc-2022-223
Preprint. Discussion started: 1 December 2022

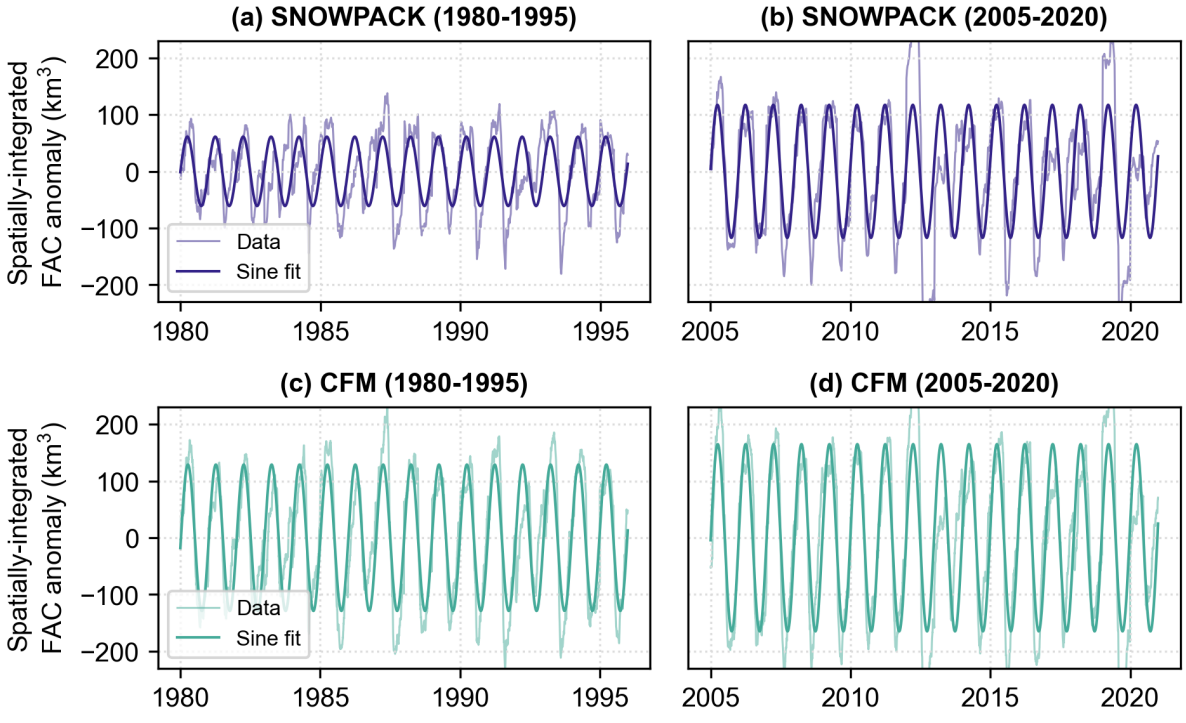

Figure A3. The seasonal breathing signal in spatially-integrated weekly firn air content (FAC) for the full ice sheet. (a) SNOWPACK seasonal signal during the 1980–1995 period, (b) SNOWPACK seasonal signal during the 2005–2020 period, (c) the CFM seasonal signal during the 1980–1995 period, (d) the CFM seasonal signal during the 2005–2020 period. The thinner lines show the anomaly, which is calculated by subtracting each year's mean spatially-integrated FAC from the record. The thicker lines are the best fit sine curve. The amplitudes of the sine curves represent the seasonal breathing signal. Note that the y-axis scales are the same in all four panels.

https://doi.org/10.5194/tc-2022-223
Preprint. Discussion started: 1 December 2022

Code and data availability. The NASA GSFC MERRA-2 data are available at https://disc.gsfc.nasa.gov/. The SUMup snow density subdataset can be found at https://arcticdata.io/catalog/view/doi%3A10.18739%2FA2NP1WK6M. Model code is available on GitHub; the code to run the SNOWPACK firn model is available at https://github.com/snowpack-model/snowpack and the code to run the Community Firn Model (CFM) is available at https://github.com/UWGlaciology/CommunityFirnModel. Data for the figures can be found on Zenodo at https://doi.org/10.5281/zenodo.7314072.

Author contributions. MTM and NW ran the SNOWPACK model, and CMS ran the CFM. MTM processed and analyzed observational data as well as output from both models, and led the manuscript writing. JTML and BM led the study design. All authors contributed to the writing of the manuscript.

Competing interests. The contact author has declared that none of the authors has any competing interests.

Acknowledgements. The authors acknowledge Eric Keenan for his assistance in accessing MERRA-2 data and compiling the SNOWPACK model. This work used the RMACC Summit supercomputer, which is supported by the National Science Foundation (awards ACI-1532235 and ACI-1532236), the University of Colorado Boulder, and Colorado State University. The Summit supercomputer is a joint effort of the University of Colorado Boulder and Colorado State University.

https://doi.org/10.5194/tc-2022-223
Preprint. Discussion started: 1 December 2022

References

Arthern, R. J., Vaughan, D. G., Rankin, A. M., Mulvaney, R., and Thomas, E. R.: In situ measurements of Antarctic snow compaction compared with predictions of models, Journal of Geophysical Research, 115, F03 011, https://doi.org/10.1029/2009JF001306, 2010.

Bartelt, P. and Lehning, M.: A physical SNOWPACK model for the Swiss avalanche warning Part I: numerical model, Cold Regions Science and Technology, p. 23, 2002.

Bavay, M. and Egger, T.: MeteoIO 2.4.2: a preprocessing library for meteorological data, Geoscientific Model Development, 7, 3135–3151, https://doi.org/10.5194/gmd-7-3135-2014, publisher: Copernicus GmbH, 2014.

Cooper, M. G., Smith, L. C., Rennermalm, A. K., Miège, C., Pitcher, L. H., Ryan, J. C., Yang, K., and Cooley, S. W.: Meltwater storage in low-density near-surface bare ice in the Greenland ice sheet ablation zone, The Cryosphere, 12, 955–970, https://doi.org/10.5194/tc-12-955-2018, 2018.

Culberg, R., Schroeder, D. M., and Chu, W.: Extreme melt season ice layers reduce firn permeability across Greenland, Nature Communications, 12, 2336, https://doi.org/10.1038/s41467-021-22656-5, 2021.

de la Peña, S., Howat, I. M., Nienow, P. W., van den Broeke, M. R., Mosley-Thompson, E., Price, S. F., Mair, D., Noël, B., and Sole, A. J.: Changes in the firn structure of the western Greenland Ice Sheet caused by recent warming, The Cryosphere, 9, 1203–1211, https://doi.org/10.5194/tc-9-1203-2015, 2015.

Dunmire, D., Lenaerts, J. T. M., Banwell, A. F., Wever, N., Shragge, J., Lhermitte, S., Drews, R., Pattyn, F., Hansen, J. S. S., Willis, I. C., Miller, J., and Keenan, E.: Observations of Buried Lake Drainage on the Antarctic Ice Sheet, Geophysical Research Letters, 47, e2020GL087 970, https://doi.org/10.1029/2020GL087970, 2020.

Dunmire, D., Banwell, A. F., Wever, N., Lenaerts, J. T. M., and Datta, R. T.: Contrasting regional variability of buried meltwater extent over 2 years across the Greenland Ice Sheet, The Cryosphere, 15, 2983–3005, https://doi.org/10.5194/tc-15-2983-2021, 2021.

Enderlin, E. M., Howat, I. M., Jeong, S., Noh, M.-J., van Angelen, J. H., and van den Broeke, M. R.: An improved mass budget for the Greenland ice sheet, Geophysical Research Letters, 41, 866–872, https://doi.org/10.1002/2013GL059010, 2014.

Forster, R. R., Box, J. E., van den Broeke, M. R., Miège, C., Burgess, E. W., van Angelen, J. H., Lenaerts, J. T. M., Koenig, L. S., Paden, J., Lewis, C., Gogineni, S. P., Leuschen, C., and McConnell, J. R.: Extensive liquid meltwater storage in firn within the Greenland ice sheet, Nature Geoscience, 7, 95–98, https://doi.org/10.1038/ngeo2043, bandiera_abtest: a Cg_type: Nature Research Journals Number: 2 Primary_atype: Research Publisher: Nature Publishing Group Subject_term: Climate-change impacts;Cryospheric science;Hydrology Subject_term_id: climate-change-impacts;cryospheric-science;hydrology, 2014.

Gelaro, R., McCarty, W., Suárez, M. J., Todling, R., Molod, A., Takacs, L., Randles, C. A., Darmenov, A., Bosilovich, M. G., Reichle, R., Wargan, K., Coy, L., Cullather, R., Draper, C., Akella, S., Buchard, V., Conaty, A., Silva, A. M. d., Gu, W., Kim, G.-K., Koster, R., Lucchesi, R., Merkova, D., Nielsen, J. E., Partyka, G., Pawson, S., Putman, W., Rienecker, M., Schubert, S. D., Sienkiewicz, M., and Zhao, B.: The Modern-Era Retrospective Analysis for Research and Applications, Version 2 (MERRA-2), Journal of Climate, 30, 5419–5454, https://doi.org/10.1175/JCLI-D-16-0758.1, 2017.

Global Modeling and Assimilation Office (GMAO): MERRA-2 tavg1_2d_rad_Nx: 2d,1-Hourly,Time-Averaged,Single-Level,Assimilation,Radiation Diagnostics V5.12.4, Greenbelt, MD, USA, Goddard Earth Sciences Data and Information Services Center (GES DISC), https://doi.org/10.5067/Q9QMY5PBNV1T, type: dataset, 2015a.

Global Modeling and Assimilation Office (GMAO): MERRA-2 tavg1_2d_int_Nx: 2d,1-Hourly,Time-Averaged,Single-Level,Assimilation,Vertically Integrated Diagnostics V5.12.4, Greenbelt, MD, USA, Goddard Earth Sciences Data and Information Services Center (GES DISC), https://doi.org/10.5067/Q5GVUVUIVGO7, type: dataset, 2015b.

Global Modeling and Assimilation Office (GMAO): MERRA-2 tavg1_2d_flx_Nx: 2d,1-Hourly,Time-Averaged,Single-Level,Assimilation,Surface Flux Diagnostics V5.12.4, Greenbelt, MD, USA, Goddard Earth Sciences Data and Information Services Center (GES DISC), https://doi.org/10.5067/7MCPBJ41Y0K6, type: dataset, 2015c.

Global Modeling and Assimilation Office (GMAO): MERRA-2 tavg1_2d_slv_Nx: 2d,1-Hourly,Time-Averaged,Single-Level,Assimilation,Single-Level Diagnostics V5.12.4, Greenbelt, MD, USA, Goddard Earth Sciences Data and Information Services Center (GES DISC), https://doi.org/10.5067/VJAFPLI1CSIV, type: dataset, 2015d.

Harper, J., Humphrey, N., Pfeffer, W. T., Brown, J., and Fettweis, X.: Greenland ice-sheet contribution to sea-level rise buffered by meltwater storage in firn, Nature, 491, 240–243, https://doi.org/10.1038/nature11566, 2012.

Herron, M. M. and Langway, C. C.: Firn Densification: An Empirical Model, Journal of Glaciology, 25, 373–385, https://doi.org/10.3189/S0022143000015239, 1980.

Izeboud, M., Lhermitte, S., Van Tricht, K., Lenaerts, J. T. M., Van Lipzig, N. P. M., and Wever, N.: The Spatiotemporal Variability of Cloud Radiative Effects on the Greenland Ice Sheet Surface Mass Balance, Geophysical Research Letters, 47, e2020GL087 315, https://doi.org/10.1029/2020GL087315, 2020.

Keenan, E., Wever, N., Dattler, M., Lenaerts, J. T. M., Medley, B., Kuipers Munneke, P., and Reijmer, C.: Physics-based SNOWPACK model improves representation of near-surface Antarctic snow and firn density, The Cryosphere, 15, 1065–1085, https://doi.org/10.5194/tc-15-1065-2021, 2021.

Lehning, M., Bartelt, P., Brown, B., and Fierz, C.: A physical SNOWPACK model for the Swiss avalanche warning Part III: meteorological forcing, thin layer formation and evaluation, Cold Regions Science and Technology, p. 16, 2002a.

Lehning, M., Bartelt, P., Brown, B., Fierz, C., and Satyawali, P.: A physical SNOWPACK model for the Swiss avalanche warning Part II. Snow microstructure, Cold Regions Science and Technology, p. 21, 2002b.

Li, J. and Zwally, H. J.: Modeling of firn compaction for estimating ice-sheet mass change from observed ice-sheet elevation change, Annals of Glaciology, 52, 1–7, https://doi.org/10.3189/172756411799096321, publisher: Cambridge University Press, 2011.

Ligtenberg, S. R. M., Helsen, M. M., and van den Broeke, M. R.: An improved semi-empirical model for the densification of Antarctic firn, The Cryosphere, 5, 809–819, https://doi.org/10.5194/tc-5-809-2011, 2011.

Ligtenberg, S. R. M., Horwath, M., van den Broeke, M. R., and Legrésy, B.: Quantifying the seasonal "breathing" of the Antarctic ice sheet, Geophysical Research Letters, 39, https://doi.org/10.1029/2012GL053628, 2012.

Ligtenberg, S. R. M., Kuipers Munneke, P., Noël, B. P. Y., and van den Broeke, M. R.: Brief communication: Improved simulation of the present-day Greenland firn layer (1960–2016), The Cryosphere, 12, 1643–1649, https://doi.org/10.5194/tc-12-1643-2018, 2018.

Lundin, J. M., Stevens, C. M., Arthern, R., Buizert, C., Orsi, A., Ligtenberg, S. R., Simonsen, S. B., Cummings, E., Essery, R., Leahy, W., Harris, P., Helsen, M. M., and Waddington, E. D.: Firn Model Intercomparison Experiment (FirnMICE), Journal of Glaciology, 63, 401–422, https://doi.org/10.1017/jog.2016.114, 2017.

MacFerrin, M., Machguth, H., As, D. v., Charalampidis, C., Stevens, C. M., Heilig, A., Vandecrux, B., Langen, P. L., Mottram, R., Fettweis, X., Broeke, M. R. v. d., Pfeffer, W. T., Moussavi, M. S., and Abdalati, W.: Rapid expansion of Greenland's low-permeability ice slabs, Nature, 573, 403–407, https://doi.org/10.1038/s41586-019-1550-3, 2019.

MacFerrin, M. J., Stevens, C. M., Vandecrux, B., Waddington, E. D., and Abdalati, W.: The Greenland Firn Compaction Verification and Reconnaissance (FirnCover) dataset, 2013–2019, Earth System Science Data, 14, 955–971, https://doi.org/10.5194/essd-14-955-2022, 2022.

Machguth, H., MacFerrin, M., van As, D., Box, J. E., Charalampidis, C., Colgan, W., Fausto, R. S., Meijer, H. A. J., Mosley-Thompson, E., and van de Wal, R. S. W.: Greenland meltwater storage in firn limited by near-surface ice formation, Nature Climate Change, 6, 390–393, https://doi.org/10.1038/nclimate2899, 2016.

Medley, B., Neumann, T. A., Zwally, H. J., Smith, B. E., and Stevens, C. M.: Simulations of firn processes over the Greenland and Antarctic ice sheets: 1980–2021, The Cryosphere, 16, 3971–4011, https://doi.org/10.5194/tc-16-3971-2022, 2022.

Michlmayr, G., Lehning, M., Koboltschnig, G., Holzmann, H., Zappa, M., Mott, R., and Schöner, W.: Application of the Alpine 3D model for glacier mass balance and glacier runoff studies at Goldbergkees, Austria, Hydrological Processes, 22, 3941–3949, https://doi.org/10.1002/hyp.7102, _eprint: https://onlinelibrary.wiley.com/doi/pdf/10.1002/hyp.7102, 2008.

Miller, O., Solomon, D. K., Miège, C., Koenig, L., Forster, R., Schmerr, N., Ligtenberg, S. R. M., and Montgomery, L.: Direct Evidence of Meltwater Flow Within a Firn Aquifer in Southeast Greenland, Geophysical Research Letters, 45, 207–215, https://doi.org/10.1002/2017GL075707, 2018.

Montgomery, L., Koenig, L., and Alexander, P.: The SUMup dataset: compiled measurements of surface mass balance components over ice sheets and sea ice with analysis over Greenland, Earth System Science Data, 10, 1959–1985, https://doi.org/10.5194/essd-10-1959-2018, 2018.

Moon, T., Fisher, M., Harden, L., Simonoko, H., and Stafford, T.: QGreenland (v2.0.0), National Snow and Ice Data Center, 2022.

Morlighem, M., Williams, C. N., Rignot, E., An, L., Arndt, J. E., Bamber, J. L., Catania, G., Chauché, N., Dowdeswell, J. A., Dorschel, B., Fenty, I., Hogan, K., Howat, I., Hubbard, A., Jakobsson, M., Jordan, T. M., Kjeldsen, K. K., Millan, R., Mayer, L., Mouginot, J., Noël, B. P. Y., O'Cofaigh, C., Palmer, S., Rysgaard, S., Seroussi, H., Siegert, M. J., Slabon, P., Straneo, F., van den Broeke, M. R., Weinrebe, W., Wood, M., and Zinglersen, K. B.: BedMachine v3: Complete Bed Topography and Ocean Bathymetry Mapping of Greenland From Multibeam Echo Sounding Combined With Mass Conservation, Geophysical Research Letters, 44, 11,051–11,061, https://doi.org/10.1002/2017GL074954, _eprint: https://onlinelibrary.wiley.com/doi/pdf/10.1002/2017GL074954, 2017.

Nash, J. E. and Sutcliffe, J. V.: River flow forecasting through conceptual models part I — A discussion of principles, Journal of Hydrology, 10, 282–290, https://doi.org/10.1016/0022-1694(70)90255-6, 1970.

Pfeffer, W. T., Meier, M. F., and Illangasekare, T. H.: Retention of Greenland runoff by refreezing: Implications for projected future sea level change, Journal of Geophysical Research: Oceans, 96, 22 117–22 124, https://doi.org/10.1029/91JC02502, 1991.

Rennermalm, A. K., Hock, R., Covi, F., Xiao, J., Corti, G., Kingslake, J., Leidman, S. Z., Miège, C., Macferrin, M., Machguth, H., Osterberg, E., Kameda, T., and McConnell, J. R.: Shallow firn cores 1989–2019 in southwest Greenland's percolation zone reveal decreasing density and ice layer thickness after 2012, Journal of Glaciology, pp. 1–12, https://doi.org/10.1017/jog.2021.102, 2021.

Rignot, E. and Mouginot, J.: Ice flow in Greenland for the International Polar Year 2008–2009, Geophysical Research Letters, 39, https://doi.org/10.1029/2012GL051634, 2012.

Smith, B. E., Medley, B., Fettweis, X., Sutterley, T., Alexander, P., Porter, D., and Tedesco, M.: Evaluating Greenland Surface-Mass-Balance and Firn-Densification Data Using ICESat-2 Altimetry, preprint, Ice sheets/Mass Balance Obs, https://tc.copernicus.org/preprints/tc-2022-44/, 2022.

Steger, C. R., Reijmer, C. H., van den Broeke, M. R., Wever, N., Forster, R. R., Koenig, L. S., Kuipers Munneke, P., Lehning, M., Lhermitte, S., Ligtenberg, S. R. M., Miège, C., and Noël, B. P. Y.: Firn Meltwater Retention on the Greenland Ice Sheet: A Model Comparison, Frontiers in Earth Science, 5, 3, https://doi.org/10.3389/feart.2017.00003, 2017.

Stevens, C. M., Verjans, V., Lundin, J. M. D., Kahle, E. C., Horlings, A. N., Horlings, B. I., and Waddington, E. D.: The Community Firn Model (CFM) v1.0, Geoscientific Model Development, 13, 4355–4377, https://doi.org/10.5194/gmd-13-4355-2020, 2020.

Tedstone, A. J. and Machguth, H.: Increasing surface runoff from Greenland's firn areas, Nature Climate Change, 12, 672–676, https://doi.org/10.1038/s41558-022-01371-z, number: 7 Publisher: Nature Publishing Group, 2022.

Thompson-Munson, M., Montgomery, L., Lenaerts, J., and Koenig, L.: Surface Mass Balance and Snow Depth on Sea Ice Working Group (SUMup) snow density subdataset, Greenland and Antartica, 1952-2019, Arctic Data Center, https://doi.org/10.18739/A24Q7QR58, 2022.

van Angelen, J. H., M. Lenaerts, J. T., van den Broeke, M. R., Fettweis, X., and van Meijgaard, E.: Rapid loss of firn pore space accelerates 21st century Greenland mass loss, Geophysical Research Letters, 40, 2109–2113, https://doi.org/10.1002/grl.50490, 2013.

van den Broeke, M., Bamber, J., Ettema, J., Rignot, E., Schrama, E., van de Berg, W. J., van Meijgaard, E., Velicogna, I., and Wouters, B.: Partitioning Recent Greenland Mass Loss, Science, 326, 984–986, https://doi.org/10.1126/science.1178176, 2009.

van Kampenhout, L., Rhoades, A. M., Herrington, A. R., Zarzycki, C. M., Lenaerts, J. T. M., Sacks, W. J., and van den Broeke, M. R.: Regional grid refinement in an Earth system model: impacts on the simulated Greenland surface mass balance, The Cryosphere, 13, 1547–1564, https://doi.org/10.5194/tc-13-1547-2019, publisher: Copernicus GmbH, 2019.

Van Tricht, K., Lhermitte, S., Lenaerts, J. T. M., Gorodetskaya, I. V., L'Ecuyer, T. S., Noël, B., van den Broeke, M. R., Turner, D. D., and van Lipzig, N. P. M.: Clouds enhance Greenland ice sheet meltwater runoff, Nature Communications, 7, 10 266, https://doi.org/10.1038/ncomms10266, 2016.

Vandecrux, B., MacFerrin, M., Machguth, H., Colgan, W. T., van As, D., Heilig, A., Stevens, C. M., Charalampidis, C., Fausto, R. S., Morris, E. M., Mosley-Thompson, E., Koenig, L., Montgomery, L. N., Miège, C., Simonsen, S. B., Ingeman-Nielsen, T., and Box, J. E.: Firn data compilation reveals widespread decrease of firn air content in western Greenland, The Cryosphere, 13, 845–859, https://doi.org/10.5194/tc-13-845-2019, 2019.

Vandecrux, B., Fausto, R. S., van As, D., Colgan, W., Langen, P. L., Haubner, K., Ingeman-Nielsen, T., Heilig, A., Stevens, C. M., MacFerrin, M., Niwano, M., Steffen, K., and Box, J.: Firn cold content evolution at nine sites on the Greenland ice sheet between 1998 and 2017, Journal of Glaciology, 66, 591–602, https://doi.org/10.1017/jog.2020.30, 2020a.

Vandecrux, B., Mottram, R., Langen, P. L., Fausto, R. S., Olesen, M., Stevens, C. M., Verjans, V., Leeson, A., Ligtenberg, S., Kuipers Munneke, P., Marchenko, S., van Pelt, W., Meyer, C. R., Simonsen, S. B., Heilig, A., Samimi, S., Marshall, S., Machguth, H., MacFerrin, M., Niwano, M., Miller, O., Voss, C. I., and Box, J. E.: The firn meltwater Retention Model Intercomparison Project (RetMIP): evaluation of nine firn models at four weather station sites on the Greenland ice sheet, The Cryosphere, 14, 3785–3810, https://doi.org/10.5194/tc-14-3785-2020, 2020b.

Vionnet, V., Brun, E., Morin, S., Boone, A., Faroux, S., Le Moigne, P., Martin, E., and Willemet, J.-M.: The detailed snowpack scheme Crocus and its implementation in SURFEX v7.2, Geoscientific Model Development, 5, 773–791, https://doi.org/10.5194/gmd-5-773-2012, publisher: Copernicus GmbH, 2012.

Wever, N., Keenan, E., Amory, C., Lehning, M., Sigmund, A., Huwald, H., and Lenaerts, J. T. M.: Observations and simulations of new snow density in the drifting snow dominated environment of Antarctica, Journal of Glaciology, accepted, 2022.

Wilhelms, F.: Density of ice core ngt03C93.2 from the North Greenland Traverse, PANGAEA, https://doi.org/10.1594/PANGAEA.56560, publisher: PANGAEA Type: dataset, 2000.

https://doi.org/10.5194/tc-2022-223
Preprint. Discussion started: 1 December 2022

Zhang, W., Wang, Y., Smeets, P. C. J. P., Reijmer, C. H., Huai, B., Wang, J., and Sun, W.: Estimating near-surface climatology of multi-reanalyses over the Greenland Ice Sheet, Atmospheric Research, 259, 105 676, https://doi.org/10.1016/j.atmosres.2021.105676, 2021.